

## CHAPTER 4

# FLOW PATTERNS AND WALL SHEAR STRESS IN ARTERIES

## *II CURVED TUBES*

We now turn to the second main feature of the thoracic aorta: its curvature. The aim is to describe flow near the entrance of a curved tube in the same way that the previous section described flow near the entrance of a straight tube. However, we immediately come up against the major difficulty that the fully developed flow to which the entry flow tends, and which in a straight tube is Poiseuille flow (the mean flow) plus an easily calculated oscillatory component, is very complicated, and even the steady component is not yet completely understood. In the next three sections, therefore, we concentrate on fully developed flow in curved tubes, leaving a discussion of entry flow to §§ 4.4 and 4.5.

The reason why the flow in a curved tube is difficult to calculate lies in the fact that the motion cannot be everywhere parallel to the curved axis of the tube, but transverse (or secondary) components of velocity must be present. This follows because in order for a fluid particle to travel in a curved path of radius  $R$  with speed  $w$  it must be acted on by a lateral force (provided by the pressure gradients in the fluid) to give it a lateral acceleration  $w^2/R$ . Now the pressure gradient acting on all particles will be approximately uniform, but the velocity of those particles near the wall will be much lower than that of particles in the core, as a result of the no-slip condition. Therefore the radius of curvature of the path of particles in the core must be greater than that of particles near the wall. In other words, fluid in the core is swept to the outside of the bend, and that near the wall returns towards the inside; a secondary circulation, like that depicted in fig. 4.1, is set up. These secondary motions themselves influence the distribution of axial velocity and result in a complicated interaction of the two.

We begin by writing down the full equations of motion for unsteady viscous flow in a curved tube, without yet imposing the

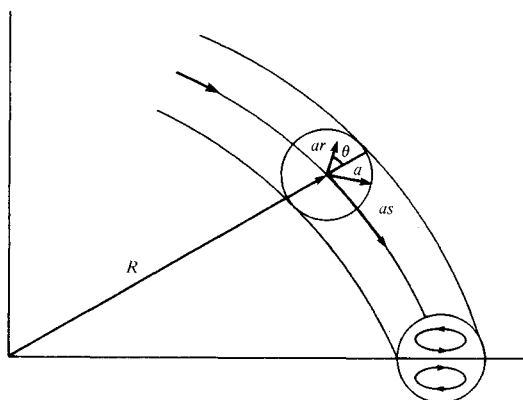


Fig. 4.1. Coordinate system to be used in analysing flow in curved tubes ( $a$  is the radius of the tube,  $R$  is the radius of curvature of the axis). A qualitative sketch of the secondary motions to be expected in steady flow is included.

restriction that the flow should be fully developed. We also retain the possibility that the curvature of the centre line is non-uniform, although we do restrict it to lie in a single plane. It is not difficult, but is even more cumbersome, to include the effect of torsion (Farthing, 1977). Coordinates  $(ar, \theta, as)$  are chosen, where  $a$  is the radius of the tube cross-section, assumed uniform (so the tube boundary is  $r = 1$ );  $as$  is the distance measured along the centre line (equivalent to  $\hat{x}$  in the straight tube considered in chapter 3), and  $(ar, \theta)$  are polar coordinates in the cross-section. We take the velocity field to be  $\hat{W}_0(u, v, w)$ , where  $\hat{W}_0$  is a suitable velocity-scale, so that the dimensionless longitudinal velocity is  $w$ , not  $u$  as heretofore; this is done so that the present notation should be consistent with that of the other authors referred to subsequently. Let the radius of curvature of the centre line at a particular cross-section be  $R$ , and define the dimensionless ratio  $\delta(s) = a/R$ , which depends on  $s$  if  $R$  is not uniform. Finally, we define the parameter

$$h = 1 + \delta(s)r \cos \theta,$$

which is  $1/R$  times the distance from the centre of curvature of the centre line (at a particular  $s$ ) to the projection on the plane containing the centre line of a general point  $(r, \theta, s)$ . In this

orthogonal coordinate system, the continuity equation  $\text{div } \mathbf{u} = 0$  is

$$u_r + \frac{u(1+2\delta r \cos \theta)}{rh} + \frac{v_\theta}{r} - \frac{v\delta \sin \theta}{h} + \frac{w_s}{h} = 0, \quad (4.1)$$

and the three momentum equations are:

$$\begin{aligned} u_t + uu_r + \frac{v}{r}u_\theta + \frac{w}{h}u_s - \frac{v^2}{r} - \frac{\delta \cos \theta}{h}w^2 \\ = -p_r + \frac{Re^{-1}}{rh} \left\{ \frac{\partial}{\partial s} \left[ \frac{r}{h} (u_s - hw_r - \delta \cos \theta w) \right] \right. \\ \left. - \frac{\partial}{\partial \theta} \left[ h \left( v_r + \frac{v}{r} - \frac{u_\theta}{r} \right) \right] \right\}, \end{aligned} \quad (4.2)$$

$$\begin{aligned} v_t + uv_r + \frac{v}{r}v_\theta + \frac{w}{h}v_s + \frac{uv}{r} + \frac{\delta \sin \theta}{h}w^2 \\ = -\frac{1}{r}p_\theta + \frac{Re^{-1}}{h} \left\{ \frac{\partial}{\partial r} \left[ h \left( v_r + \frac{v}{r} - \frac{u_\theta}{r} \right) \right] \right. \\ \left. - \frac{\partial}{\partial s} \left[ \frac{1}{rh} (hw_\theta - \delta r \sin \theta w - rv_s) \right] \right\}, \end{aligned} \quad (4.3)$$

$$\begin{aligned} w_t + uw_r + \frac{v}{r}w_\theta + \frac{w}{h}w_s + \frac{\delta \cos \theta}{h}uw - \frac{\delta \sin \theta}{h}vw \\ = -\frac{1}{h}p_s + \frac{Re^{-1}}{r} \left\{ \frac{\partial}{\partial \theta} \left[ \frac{1}{rh} (hw_\theta - \delta r \sin \theta w - rv_s) \right] \right. \\ \left. - \frac{\partial}{\partial r} \left[ \frac{r}{h} (u_s - hw_r - \delta \cos \theta w) \right] \right\}. \end{aligned} \quad (4.4)$$

The time has been non-dimensionalised with respect to  $a/\hat{W}_0$  and the pressure with respect to  $\rho \hat{W}_0^2$ ; the Reynolds number  $Re = \hat{W}_0 a / \nu$ . These equations will be used in § 4.2 as well as in this section.

In the next three subsections we shall consider: (i) Steady fully developed flow in a tube with small curvature ( $\delta \ll 1$ ); most of the section will also assume that  $\delta$  is uniform so that the velocity field  $\mathbf{u}$

and pressure gradient ( $-\partial p/\partial s$ ) are both independent of  $s$ . When  $\delta$  is allowed to vary, it is supposed to do so on a length-scale large compared with  $a$ , so  $\partial/\partial s = O(\varepsilon) \ll 1$ . (ii) Fully developed flow with an oscillatory mean pressure gradient,  $\delta \ll 1$  and  $\delta$  uniform (so  $\partial \mathbf{u}/\partial s = 0$ ). (iii) Unsteady flow starting from rest with a given waveform of average axial velocity; here either  $\delta$  is uniform and not necessarily much less than 1, or is much less than 1 but need not be uniform ( $\partial/\partial s = O(\varepsilon)$ ). When  $\delta$  is uniform, and hence the velocity field independent of  $s$ , the only way that the transverse velocities are affected by the axial velocity is through the ‘centrifugal force’ terms that drive it; these are the last terms on the left-hand sides of (4.2) and (4.3), proportional to  $\delta w^2$ . The axial velocity is itself influenced by the transverse motions through the convective inertia terms in (4.4).

In §§ 4.1 and 4.2 it is convenient to take the velocity-scale  $\hat{W}_0$  equal to  $\nu/a$ , so  $Re = 1$ . In §§ 4.3–4.5,  $\hat{W}_0$  is an actual order of magnitude for the axial velocity; there we take  $Re \gg 1$ .

#### 4.1 Fully developed steady flow, $\delta \ll 1$

In the case where  $\delta$  is uniform and hence the velocity field independent of  $s$ , (4.4) shows that the pressure gradient  $-p_s$  is independent of  $s$ . Thus the pressure can be written in the form  $-Gs + p'(r, \theta)$ ; from (4.2) and (4.3)  $G$  is seen to be independent of  $r$  and  $\theta$  and is therefore a constant. When  $\delta$  is not uniform, but  $\partial/\partial s = O(\varepsilon) \ll 1$ , we write  $-p_s = G - \varepsilon p_s'''$ . We also set  $\delta \ll 1$  and neglect all terms that are  $O(\delta)$  or  $O(\varepsilon^2)$  compared with the leading term in any equation. First, however, we rescale  $w$  so that the centrifugal force terms in (4.2) and (4.3) are of the same order of magnitude as the viscous and inertial terms (this is necessary because the centrifugal force terms *drive* the secondary motion). To this end we replace  $w$  by  $(2\delta)^{-1/2} w'$  (the factor of  $2^{-1/2}$  is introduced for consistency with other authors); we also replace  $s$  by  $s/\varepsilon$ . Equations (4.1)–(4.4) with  $Re = 1$  then reduce to

$$u_r + \frac{u}{r} + \frac{v_\theta}{r} + \varepsilon (2\delta)^{-1/2} w'_s = 0, \quad (4.5)$$

$$\begin{aligned}
uu_r + \frac{v}{r}u_\theta - \frac{v^2}{r} - \frac{1}{2}w'^2 \cos \theta + \varepsilon(2\delta)^{-1/2}w'u_s \\
= -p'_r - \frac{1}{r} \frac{\partial}{\partial \theta} \left( v_r + \frac{v}{r} - \frac{u_\theta}{r} \right) - \varepsilon(2\delta)^{-1/2}w'_{rs}, \quad (4.6)
\end{aligned}$$

$$\begin{aligned}
uv_r + \frac{v}{r}v_\theta + \frac{uv}{r} + \frac{1}{2}w'^2 \sin \theta + \varepsilon(2\delta)^{-1/2}w'v_s \\
= -\frac{1}{r}p'_\theta + \frac{\partial}{\partial r} \left( v_r + \frac{v}{r} - \frac{u_\theta}{r} \right) - \varepsilon(2\delta)^{-1/2} \frac{w'_{\theta s}}{r}, \quad (4.7)
\end{aligned}$$

$$\begin{aligned}
uw'_r + \frac{v}{r}w'_\theta + \varepsilon(2\delta)^{-1/2}w'w'_s \\
= D - \varepsilon(2\delta)^{-1/2}p''_s + \left( w'_r + \frac{1}{r}w'_r + \frac{1}{r^2}w'_\theta \right). \quad (4.8)
\end{aligned}$$

The boundary conditions are that  $u = v = w' = 0$  on  $r = 1$ , and that there should be no singularity at  $r = 0$ .

In the last equation  $p''_s = 2\delta p'''_s$ , and the parameter  $D$  is given by

$$D = (2\delta)^{1/2}G = (2\delta)^{1/2} \frac{\hat{G}a^2}{\mu} \cdot \frac{a}{\nu}, \quad (4.9)$$

where  $-\hat{G}$  is the dimensional pressure gradient.  $\hat{G}a^2/\mu$  is four times the peak velocity in Poiseuille flow in a straight tube, driven by the same pressure gradient  $-\hat{G}$ , so  $D = (2\delta)^{1/2} \cdot 4Re'$ , where  $Re'$  is the Reynolds number of the straight-tube flow.  $D$  is called the Dean number, because Dean (1928) was the first to realise its significance in curved-tube flow.

When the curvature is uniform ( $\varepsilon = 0$ ), the flow is entirely governed by the single dimensionless parameter  $D$ ; a slow variation in curvature will have a small effect on the flow as long as  $\varepsilon' = \varepsilon(2\delta)^{-1/2} \ll 1$ . We shall examine the flow with  $\varepsilon' = 0$ , (a) for small  $D$  (an analytical solution), (b) for a wide range of  $D$ , becoming quite large (numerical solutions), and (c) for very large  $D$  (an incomplete asymptotic theory). In (a) we shall also briefly examine the consequences of a non-zero, but small,  $\varepsilon'$ . When  $\varepsilon' = 0$ , the continuity equation, (4.5), admits of the existence of a secondary stream function,  $\psi$ , such that

$$u = (1/r)\psi_\theta, \quad v = -\psi_r, \quad (4.10)$$

and then the other equations reduce to the pair of coupled equations:

$$\nabla_1^2 w' + D = (1/r)(\psi_\theta w'_r - \psi_r w'_\theta), \quad (4.11)$$

$$\nabla_1^4 \psi + \frac{1}{r} \left( \psi_r \frac{\partial}{\partial \theta} - \psi_\theta \frac{\partial}{\partial r} \right) \nabla_1^2 \psi = -w' \left( \sin \theta w'_r + \frac{\cos \theta}{r} w'_\theta \right), \quad (4.12)$$

where

$$\nabla_1^2 \equiv \partial^2 / \partial r^2 + (1/r) \partial / \partial r + (1/r^2) \partial^2 / \partial \theta^2.$$

The boundary conditions at  $r = 1$  are  $\psi = \psi_r = w' = 0$ .

#### 4.1.1 Small $D$

Dean (1928) gave the first few terms of a series solution of (4.11) and (4.12) in powers of  $D$ ; the leading term for  $w'$  ( $=O(D)$ ) is just Poiseuille flow in a straight tube, and the leading term for  $\psi$  is  $O(D^2)$  from (4.12). The procedure is equivalent to the successive approximation of inertia terms in lubrication theory, only the lubrication theory is particularly simple because the cross-sectional area of the tube is uniform. If we set

$$w' = D \sum_{n=0}^{\infty} D^{2n} w_n(r, \theta), \quad \psi = \sum_{n=1}^{\infty} D^{2n} \psi_n(r, \theta),$$

then

$$\left. \begin{aligned} w_0 &= \frac{1}{4}(1-r^2), \\ \psi_1 &= [2 \sin \theta / (9 \times 8^3)] r(1-\frac{1}{4}r^2)(1-r^2)^2, \\ w_1 &= [\cos \theta / (45 \times 8^5)] r(1-r^2)(19-21r^2+9r^4-r^6), \end{aligned} \right\} \quad (4.13)$$

etc. Dean's main application was to calculate the dimensionless flow rate,  $Q$ , corresponding to a particular value of  $D$ . The term  $w_1$  does not contribute to it, and, in fact, Dean calculated the contributions from all the terms up to  $O(D^9)$  (i.e.  $w_4$ ) to obtain

$$\begin{aligned} Q &= \int_0^{2\pi} \int_0^1 w' r \, dr \, d\theta \\ &= (\pi D/8)[1 - 0.0306(D/96)^4 + 0.0120(D/96)^8 + O(D^{12})], \end{aligned}$$

where  $\frac{1}{8}\pi D$  is the Poiseuille flow value in the present scaled variables. The size of the coefficients in this series suggests that the

small- $D$  expansion is valid for values of  $D$  up to about 100. In the canine aorta, however, where  $\delta \approx 0.2$  and the mean Reynolds number is approximately 800, the mean value of  $D$  is greater than 2000 (and the peak value is greater still), so this expansion can be useful only for much smaller blood vessels. Note that the leading term in the secondary flow, represented by  $\psi_1$  in (4.13), takes the form of a pair of vortices, as shown schematically in fig. 4.1 (see also fig. 4.2). They are symmetrical about  $\theta = \pm \frac{1}{2}\pi$ , and the flow is towards the outside of the curve ( $\theta = 0$ ) in the core of the tube and towards the inside near the walls.

The effect of non-uniform curvature can be assessed in a similar way when  $\delta \ll \varepsilon' \ll 1$ . We calculate merely the first-order correction to  $u_1$ ,  $v_1$  and  $w_1$ . If we suppose that the  $\delta$  used in the change of variables leading to (4.5)–(4.8) is a constant,  $\delta_0$ , then the fact that  $\delta$  is a function of  $s$  appears only in the two centrifugal force terms on the left-hand sides of (4.6) and (4.7), involving  $w'^2$ ; these terms should be multiplied by  $\Delta(s) = \delta(s)/\delta_0 = O(1)$ . Then the solution with  $\varepsilon' = 0$  is altered only in that  $w_1$ ,  $\psi_1$  are multiplied by  $\Delta(s)$  etc.;  $w_0$  is unchanged. To find the first-order correction to  $u_1$ ,  $v_1$ ,  $w_1$ , write

$$\left. \begin{aligned} u &= D^2[(\Delta(s)/r)\psi_{1\theta} + \varepsilon' D\Delta'(s)u_{11}], \\ v &= D^2[-\Delta(s)\psi_{1r} + \varepsilon' D\Delta'(s)v_{11}], \\ w' &= Dw_0 + D^3[\Delta(s)w_1 + \varepsilon' D\Delta'(s)w_{11}], \end{aligned} \right\} \quad (4.14)$$

substitute into (4.5)–(4.8) and retain only the leading terms. The continuity equation, (4.5), gives

$$u_{11r} + u_{11}/r + v_{11\theta}/r = -w_1(r, \theta), \quad (4.15)$$

while the  $O(\varepsilon'D^3)$  terms in (4.6) and (4.7) can be combined to yield

$$\nabla_1^2 \Omega_{11} = (1/r)(\partial/\partial r)(rw_0 v_1) - w_0 u_{1\theta}/r, \quad (4.16)$$

where

$$\Omega_{11} = v_{11r} + v_{11}/r - u_{11\theta}/r.$$

The leading term in (4.8) yields an equation for  $w_{11}$ , as follows:

$$\nabla_1^2 w_{11} = -G_{11} + u_{11}w_{0r} + w_0 w_1, \quad (4.17)$$

where  $-\varepsilon'D^4\Delta'(s)G_{11}$  is independent of  $r$  and  $\theta$  and is the correction to the pressure gradient required to keep the volume flux

independent of  $s$ ;  $G_{11}$  is zero, in fact, because  $w_{11}$  is proportional to  $\cos \theta$ , but the corresponding term at the next order would in general not be zero. The solutions of (4.15)–(4.17) that satisfy the boundary conditions are

$$\left. \begin{aligned} u_{11} &= C \cos \theta (1-r^2)^2 f(r), \\ v_{11} &= C \sin \theta (1-r^2) g(r), \\ w_{11} &= C \cos \theta r(1-r^2) h(r), \end{aligned} \right\} \quad (4.18)$$

where

$$\left. \begin{aligned} C &= 1/(270 \times 8^5), \\ f(r) &= -13 + 15r^2 - 7r^4 + r^6, \\ g(r) &= 13 - 224r^2 + 266r^4 - 124r^6 + 17r^8, \\ h(r) &= (1/3360)(-7338 + 7362r^2 - 6498r^4 + 3903r^6 \\ &\quad - 548r^8 + 40r^{10}). \end{aligned} \right\} \quad (4.19)$$

It is to be expected that, in a tube of increasing curvature ( $\Delta' > 0$ ), there will be a delay in setting up the secondary motions, which will therefore be weaker at a given value of  $s$  than they would be in a uniformly curved tube, with  $\Delta$  equal to its value at  $s$ . The above solutions confirm this expectation, as we can see by considering the secondary motion at  $r = 0$ , where it reduces to a velocity of magnitude

$$[D^2/(9 \times 8^3)][2\Delta(s) - \varepsilon' D\Delta'(s)(13/1920)]$$

in the  $\theta = 0$  direction.

The quantity of greatest interest in the context of blood vessels is the shear stress on the vessel walls. This has two components which in non-dimensional variables are  $-w'_r|_{r=1}$  in the axial ( $s$ -) direction and  $-v_r|_{r=1}$  in the tangential ( $\theta$ -) direction. To the order of this calculation, these quantities are:

$$\begin{aligned} -w'_r|_{r=1} &= \frac{1}{2}D + [D^3 \cos \theta / (30 \times 8^4)] \\ &\quad \times [\Delta(s) - \varepsilon' D\Delta'(s)(73/3024)], \\ -v_r|_{r=1} &= [D^2 \sin \theta / (6 \times 8^2)] \\ &\quad \times [\Delta(s) - \varepsilon' D\Delta'(s)(13/5760)]. \end{aligned} \quad (4.20)$$



These results show (i) that curvature increases axial wall shear on the outside wall ( $|\theta| < \frac{1}{2}\pi$ ) and decreases it on the inside, (ii) that increasing curvature ( $\Delta' > 0$ ) diminishes this effect, (iii) that curvature generates a positive secondary shear in the  $\theta$ -direction (consistent with the qualitative diagram in fig. 4.1), and (iv) that increasing curvature reduces this secondary shear slightly (but only slightly: the numerical coefficient of  $\varepsilon'D\Delta$  in the second of equations (4.20) is about 0.0023 compared with 0.024 for that in the first equation).

Two final points to note are (v) that the 'centres' of the secondary vortices, i.e. the stagnation points on  $\theta = \pm\frac{1}{2}\pi$ , which are at  $r \approx 0.43$  for uniform curvature, are moved out slightly to  $r \approx 0.43 + (\varepsilon'D\Delta'/\Delta) \times 5.1 \times 10^{-4}$  when the curvature is increasing; and (vi) that the position of maximum axial velocity, which is at  $r \approx 2.6 \times 10^{-5}\Delta D^2$ ,  $\theta = 0$  for uniform curvature, is moved to  $r \approx 2.6 \times 10^{-5}\Delta D^2[1 - (\varepsilon'D\Delta'/\Delta) \times 0.019]$ ,  $\theta = 0$  when the curvature is variable.

Low-Dean-number flow in a tube of variable curvature has also been studied by Murata, Miyake & Inaba (1976). They obtained the same results as above, but with some extra terms arising from a less conventional non-dimensionalisation than that used here. They kept  $Re'(\propto \delta^{-1/2}D) = O(1)$  as  $\delta \rightarrow 0$ , and then gave solutions for small and for moderate  $Re'$ , whereas we have kept  $D = O(1)$  as  $\delta \rightarrow 0$ , subsequently considering the small- $D$  expansion. The extra terms, which appear on the right-hand sides of (4.6)–(4.8), constitute kinematic corrections to zero-Reynolds-number flow, and they demonstrate, for example, that when  $Re' \ll 1$  the axial flow is shifted to the inside of a bend and not to the outside, in order to minimise the rate of energy dissipation. Murata *et al.* presented solutions for  $Re'$  up to 2000, but because of their scaling this is still equivalent to small Dean number. The great merit of their paper is that they show how to develop numerical solutions of the small- $\delta$  and small- $D$  equations for arbitrarily large values of  $\varepsilon'$ , so that tubes of small, but rapidly varying, curvature can be examined.

#### 4.1.2 Intermediate $D$

Reverting now to the case of uniform curvature, we recall that the small- $D$  expansion is inadequate to describe arteries of interest such as the aorta. Equations (4.11) and (4.12) have been solved

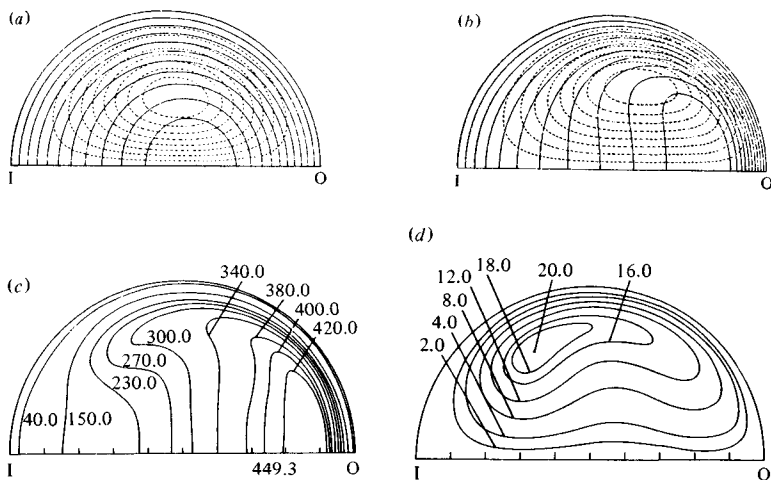


Fig. 4.2. Contour plots of axial velocity (continuous curves) and secondary streamlines (broken curves), (a)  $D = 96$ , (b)  $D = 606$ . (c) Contour plots of axial velocity,  $D = 5000$ . (d) Secondary streamlines,  $D = 5000$ . I is the inside of the bend, O the outside. (After McConalogue & Srivastava (1968) and Collins & Dennis (1975).)

numerically for values of  $D$  up to about 600 by McConalogue & Srivastava (1968), and subsequently up to  $D = 5000$  by Collins & Dennis (1975); although the methods used by these two groups were quite different, the results agree very well for  $D < 600$ . The flow pattern is depicted by plotting curves of constant  $\psi$  (secondary streamlines) and of constant  $w'$  (axial velocity contours). Results for  $D = 96$ , 606 and 5000 are shown in fig. 4.2. Fig. 4.2(a) shows that for  $D = 96$  the secondary motions are approximately symmetrical about the line  $\theta = \frac{1}{2}\pi$  (as predicted by Dean's expansion) and that the point of peak axial velocity ( $w'_{\max} = 23.4$ ) is shifted from the tube axis to about  $r = 0.20$  (compared with 0.24, which is the value predicted above by the first term in Dean's expansion). Fig. 4.2(b) shows that at the intermediate value of  $D$ , a boundary layer appears to be developing (on the outside wall of the bend) in which the axial shear is high, whereas in the core the secondary flow appears to be approximately uniform while the contours of axial velocity are approximately straight lines across the tube. This view of the axial velocity field is confirmed at  $D = 5000$  by fig. 4.2(c), but the

secondary streamlines at this value of  $D$  are quite complicated (fig. 4.2(d)), suggesting that an asymptotic theory for large  $D$  may not be straightforward. Collins & Dennis (1975) showed how well their computations agreed with experiment: figs. 4.3(a) and (b) show the agreement between the computed position and value of the maximum axial velocity and the same quantities as measured by Adler (1934), while fig. 4.3(c) shows the agreement between theoretical and experimental values of the ratio  $f(D)$  of the flow-rate in a straight tube to that in a curved tube subject to the same pressure

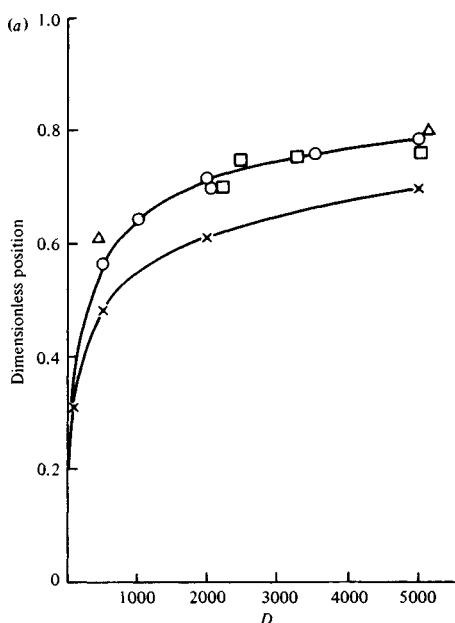
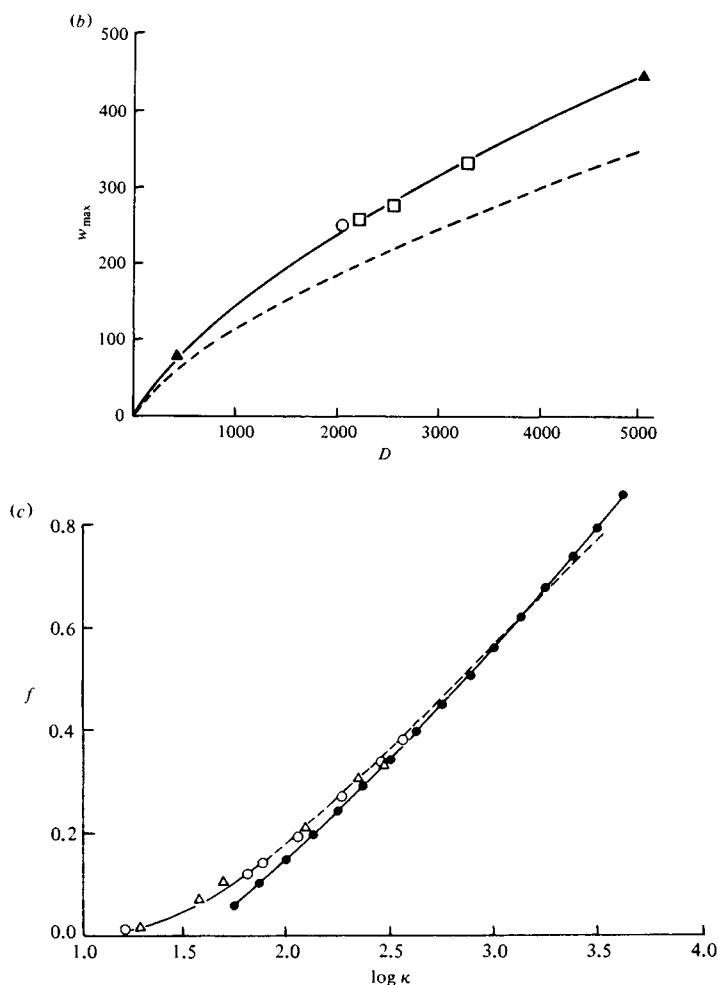


Fig. 4.3. (a) Variation of the position of maximum axial velocity along the plane of symmetry as a function of  $D$ . Numerical calculations: open circles, present theory; crosses, filled circles, open triangles, other theories. Open squares, experimental measurements of Adler (1934). (b) Magnitude of maximum dimensionless axial velocity as a function of  $D$ . Numerical calculations: continuous curve, present theory; open circles, filled triangles, broken curve, other theories. Open squares, experimental measurements of Adler (1934). (c) Variation of the friction ratio  $f$  as a function of  $\kappa$  ( $\propto D^{2/3}$ ). Numerical calculations: open circles, present theory; solid circles and curve joining them, (3.53); open triangles, continuous curve, other theories. Broken curve, experimental measurements of White (1929). (After Collins & Dennis, 1975.)

Fig. 4.3. (*continued*)

gradient. Collins & Dennis were also concerned to confirm the asymptotic structure of the solution for large  $D$ , as proposed by Ito (1969). This structure is discussed below; suffice it here to say that the numerical solutions confirmed the predicted structure in that (i)

$$f(D) \sim D^{-1/3} [a + bD^{-1/3} + O(D^{-2/3})], \quad (4.21)$$

where  $a$  and  $b$  are constants (equal to 8.12 and  $-16.7$  respectively); and that (ii)  $D^{-2/3} w'$  is approximately independent of  $D$  across the

plane of symmetry of the tube (the maximum value of  $D^{-2/3}w'$  appears to tend to a constant value around 1.6 as  $D \rightarrow \infty$ ), except near the outside wall, where (iii) there is a boundary layer of thickness proportional to  $D^{-1/3}$ , so that the wall shear,  $-w_r$  at  $r = 1$ ,  $\theta = 0$ , is proportional to  $D$  ( $\approx 0.85D$ ).

#### 4.1.3 Large $D$

The numerical results described above suggest that the structure of the solution at large  $D$  is that of an inviscid rotational core surrounded by a thin boundary layer. Suppose that a scale for the axial velocity  $w$  is  $D^\alpha$ , while a scale for  $\psi$  is  $D^\beta$  and a scale for boundary layer thickness is  $D^{-\gamma}$ . In the core, where viscous forces are negligible, the inertia terms in (4.11) must balance the driving pressure gradient  $D$ , so we must have

$$\alpha + \beta = 1.$$

In the boundary layer, however, the inertia terms in both (4.11) and (4.12) must balance the viscous terms and (in (4.12)) the centrifugal force terms. Hence

$$\beta + 4\gamma = 2\beta + 3\gamma = 2\alpha + \gamma,$$

so that  $\beta = \gamma = \frac{1}{2}\alpha = \frac{1}{3}$ . Thus we can write

$$w' = D^{2/3}\tilde{w}, \quad \psi = D^{1/3}\tilde{\psi} \quad (4.22)$$

and, in the boundary layer,

$$\zeta = D^{1/3}(1-r).$$

This scaling corresponds to that introduced at the end of the subsection for intermediate  $D$  above.

The inviscid core equations, to leading order in  $D$ , now become

$$\begin{aligned} \text{and} \quad & \tilde{w}[\sin \theta \tilde{w}_r + (\cos \theta/r)\tilde{w}_\theta] = 0 \\ & (1/r)(\tilde{\psi}_\theta \tilde{w}_r - \tilde{\psi}_r \tilde{w}_\theta) = 1, \end{aligned} \quad (4.23)$$

and their solution is

$$\tilde{w} = w_c(r \cos \theta), \quad \tilde{\psi} = r \sin \theta / w'_c(r \cos \theta), \quad (4.24)$$

where  $w_c$  is an arbitrary function of  $x = r \cos \theta$ , the Cartesian coordinate in the direction  $\theta = 0$ . The axial velocity is constant along lines of constant  $x$ , on which the secondary stream function is proportional to  $y = r \sin \theta$ .

In the boundary layer, the equations are

$$\tilde{w}_{\zeta\zeta} + \tilde{\psi}_\theta \tilde{w}_\zeta - \tilde{\psi}_\zeta \tilde{w}_\theta = 0 \quad (4.25)$$

and

$$\tilde{\psi}_{\zeta\zeta\zeta} + (\tilde{\psi}_\theta \partial/\partial\zeta - \tilde{\psi}_\zeta \partial/\partial\theta) \tilde{\psi}_{\zeta\zeta} = \sin\theta \tilde{w} \tilde{w}_\zeta, \quad (4.26a)$$

with boundary conditions

$$\left. \begin{aligned} \tilde{\psi} = \tilde{\psi}_\zeta = \tilde{w} = 0 & \quad \text{on } \zeta = 0, \\ \tilde{\psi}_\zeta \rightarrow 0, \quad \tilde{w} \rightarrow w_c(\cos\theta) & \quad \text{as } \zeta \rightarrow \infty, \\ \tilde{\psi} = \tilde{\psi}_\zeta = \tilde{w}_\theta = 0 & \quad \text{on } \theta = 0, \pi. \end{aligned} \right\} \quad (4.27)$$

Equation (4.26a) can be integrated once to give

$$\tilde{\psi}_{\zeta\zeta\zeta} + \tilde{\psi}_\theta \tilde{\psi}_{\zeta\zeta} - \tilde{\psi}_\zeta \tilde{\psi}_{\zeta\theta} = -\frac{1}{2} \sin\theta [w_c^2(\cos\theta) - \tilde{w}^2]. \quad (4.26b)$$

The boundary layer problem appears to be completely specified for any reasonable function  $w_c(\cos\theta)$ . This function is then, in principle, determined by imposing the condition that the (secondary) mass flux in the boundary layer is just enough to balance the normal inflow from the core, which is non-zero and given by  $\tilde{\psi}$  in (4.24). That is, we impose

$$\tilde{\psi}(\zeta \rightarrow \infty, \theta) = \sin\theta / w'_c(\cos\theta). \quad (4.28)$$

An apparently self-consistent approximate solution to this problem was given by Ito (1969) using the Pohlhausen momentum integral method. He was able to derive a function  $w_c(\cos\theta)$  that decreased monotonically from a given constant ( $\approx 1.9$ ) at  $\theta = 0$  to zero at  $\theta = \pi$ . Note that  $w_c(1)$  should be equal to the limit of the maximum value of  $D^{-2/3} w'$  as  $D \rightarrow \infty$ , about 1.6 according to the numerical results of Collins & Dennis (1975). The boundary layer thickness in Ito's calculations remained more or less constant until  $\theta$  was almost equal to  $\pi$ , when it increased sharply. This increase occurs because the external velocity, proportional to  $\sin\theta$ , becomes small. In fact, if we put  $\phi = \pi - \theta \ll 1$ , and suppose that near  $\phi = 0$  we have  $\psi \propto \phi^\alpha$ ,  $w' \propto \phi^\beta$  and boundary layer thickness  $\propto \phi^\gamma$ , then (4.28) implies that  $\alpha + \beta = 3$ . Balance of the viscous, inertial and centrifugal force terms in the boundary layer equation (4.26b)

then gives

$$\alpha - 3\gamma = 2\alpha - 2\gamma - 1 = 2\beta + 1,$$

from which we obtain  $\alpha = \frac{5}{3}$ ,  $\beta = \frac{4}{3}$ ,  $\gamma = -\frac{2}{3}$ . Thus the solution in the core near  $\phi = 0$  should be of the form

$$\tilde{w}_c = \sqrt{2A}\phi^{4/3}[1 + O(\phi^2)], \quad \tilde{\psi}_c = (3/4A\sqrt{2})\phi^{5/3}[1 + O(\phi^2)], \quad (4.29)$$

while that in the boundary layer should be of the form

$$\begin{aligned} \tilde{w} &= \sqrt{2A}\phi^{4/3}H(\eta)[1 + O(\phi^2)], \\ \tilde{\psi} &= A^{1/2}\phi^{5/3}F(\eta), \quad \eta = A^{1/2}\zeta\phi^{2/3}, \end{aligned} \quad (4.30)$$

where

$$\begin{aligned} F''' &= \frac{5}{3}FF'' - \frac{7}{3}F'^2 + H^2 - 1, & H'' &= \frac{5}{3}FH' - \frac{4}{3}F'H, \\ F(0) &= F'(0) = H(0) = F'(\infty) = H(\infty) - 1 = 0. \end{aligned}$$

This problem has been solved numerically by Smith (1975), who found

$$F''(0) = 1.595, \quad H'(0) = 1.265, \quad F(\infty) = 0.503.$$

This last result, together with (4.29) and (4.30), shows that  $A = 1.05$  (a different value from that quoted by Smith, because his  $D$  differs from that defined in (4.9) by a factor of  $\sqrt{2}$ ).

This analysis is important because it indicates that the asymptotic structure for large  $D$ , consisting of an inviscid core and a  $D^{-1/3}$  boundary layer, may have a self-consistent solution for virtually all  $\theta$ . In fact, the solution breaks down only in a region for which  $\phi = O(D^{-1/8})$ ,  $1 - r = O(D^{-1/4})$ , because although the boundary layer approximation is still valid there (so that  $\nabla_1^2 \approx \partial^2/\partial r^2$ ) the previously neglected terms  $D$  (in (4.11)) and  $w'w'_\theta \cos \theta/r$  (in (4.12)) become as important as the others.

Riley & Dennis (1976) and others have attempted accurate numerical solutions of the boundary layer problem defined by (4.25)–(4.28). The procedure is to guess a value of  $w_c$  at  $\theta = 0$  (e.g. the value of 1.6, derived from the full numerical solution of Collins & Dennis (1975)), and then to integrate forward in  $\theta$ . For example,

if we write

$$\begin{aligned}w_c(\cos \theta) &= \sqrt{2} \sum_{n=0}^{\infty} \theta^{2n} W_n, \\ \tilde{w}(\zeta, \theta) &= \sqrt{2} \sum_{n=0}^{\infty} \theta^{2n} W_n h_n(\zeta W_0^{1/2}), \\ \tilde{\psi}(\zeta, \theta) &= W_0^{1/2} \sum_{n=0}^{\infty} \theta^{2n+1} f_n(\zeta W_0^{1/2}),\end{aligned}$$

the following problem is obtained to leading order:

$$\left. \begin{aligned}f_0''' + f_0 f_0'' - f_0'^2 + 1 - h_0^2 &= 0, & h_0'' + f_0 h_0' &= 0, \\ f_0(0) = f_0'(0) = h_0(0) = f_0'(\infty) = h_0(\infty) - 1 &= 0.\end{aligned} \right\} \quad (4.31)$$

This was solved by Stewartson (1958), and has the properties  $f_0''(0) = 0.953$ ,  $h_0'(0) = 0.463$ ,  $f_0(\infty) = 1.33$  (see Smith, 1975). Then the condition (4.28) implies  $W_1 = -0.27/W_0^{1/2}$ , so the second problem is completely determined:

$$\begin{aligned}h_1'' + f_0 h_1' - 2f_0' h_1 + 3(W_0/W_1) f_1 h_0' &= 0, \\ f_1''' + f_0 f_1'' - 4f_0' f_1' + 3f_0'' f_1 &= -2(W_1/W_0)(1 - h_0 h_1) + \frac{1}{6}(1 - f_0^2), \\ h_1(\infty) = 1, & \quad f_1'(\infty) = 0;\end{aligned}$$

this is now linear and can also be solved numerically. Riley & Dennis (1976) preferred a finite-difference integration of the boundary layer equations to the above series solution. They proposed that the correct value of  $W_0$  is that which causes the solution to approach its asymptotic form, (4.29)–(4.30), smoothly as  $\theta \rightarrow \pi$ .

However, Riley & Dennis's numerical results were incomplete, although their iterations appeared to lead to a well-defined value of  $W_0$ , because the numerical solution of the boundary layer equations broke down for values of  $\theta$  considerably smaller than  $\pi$ . This was not because of the development of separation (despite the conclusions of Barua (1963), who wrongly imposed the condition that  $w_c'(x) = \text{constant}$ ; Ito (1969) did not predict separation), but was associated with the appearance of reversed secondary flows near the edge of the boundary layer. This is not inconsistent with the



full numerical solutions (fig. 4.2(d)), but makes forward integration of the boundary layer equations impossible, and any accurate integration very difficult. It also means that Ito's (1969) momentum integral solution, which expressly forbids reversed flow in the secondary boundary layer, is unlikely to be accurate. Thus it still has not been demonstrated conclusively that the boundary layer structure outlined above is actually correct for  $\theta < \pi - O(D^{-1/8})$ . It may, for example, be correct only for  $\theta$  less than some value  $\theta_s = \pi - O(1)$  at which separation develops, but not thereafter; if separation does develop, the core flow will be significantly affected everywhere, and a theoretical prediction of  $W_0$  would then be impossible. It is also possible that the boundary layer structure is quite incorrect: Smith (1976a) has considered curved tubes whose cross-sections have straight sides, and has proposed a plausible structure in which the flow near a flat outer wall could consist of an inviscid layer (thickness  $\sim D^{-1/6}$ ) in which the core flow turns a corner, with a thin viscous region (thickness  $\sim D^{-1/4}$ ) embedded within it to satisfy the no-slip condition. He also showed that no simple solution of the boundary layer problem is possible for a rectangular cross-section, although it is for a triangular cross-section. It is not clear whether this work is relevant to tubes with curved (in particular, circular) cross-sections, but it serves to underline the difficulty of analysing curved-tube flows for large Dean numbers.†

Although the suggested boundary layer structure is not yet certain, the fact that it has a well-behaved limit as  $\theta \rightarrow \pi$ , and the consistency between it and the quoted numerical results of Collins & Dennis (1975), suggest that it can be used with some confidence for predictions of particular quantities, such as the flow-rate (represented by  $f(D)$  in (4.21)) and the axial wall shear at the outer wall,  $-w'_r$  at  $r = 1$ ,  $\theta = 0$ , which is  $\approx 0.85D$ . The values of  $a$  and  $b$  in (4.21), as obtained by Collins & Dennis, agree closely (to within  $\frac{1}{2}\%$  and 6% respectively) with the corresponding values derived by Ito (1969) from his approximate method, which lends circumstantial support to the latter.

† See also Van Dyke (1978), where further circumstantial evidence against the boundary layer structure is adduced.

### 4.2 Fully developed oscillatory flow, $\delta \ll 1$

In this section we consider only tubes of uniform curvature, but extend the work described above to cover an axial pressure gradient ( $-p_s$  in the dimensionless equation (4.4)) that varies sinusoidally with time according to

$$-p_s = G + \alpha^2 W_0 \cos \alpha^2 t. \quad (4.32)$$

Here  $W_0$  is the (dimensionless) velocity amplitude that would be driven by such a pressure gradient in a straight pipe containing an inviscid fluid, and  $\alpha$  is Womersley's parameter (see (2.35)):  $\alpha^2 = \Omega a^2/\nu$ , where  $\Omega$  is the dimensional angular frequency of the oscillation. This class of flows has been analysed by Lyne (1971) for the case  $G = 0$ , by Smith (1975), and by Blennerhassett (1976).

A secondary stream function can be defined as in (4.10) and the governing equations corresponding to (4.11) and (4.12) are

$$\nabla_1^2 w' + D + \alpha^3 (2R_s)^{1/2} \cos \tau = (1/r)(\psi_\theta w'_r - \psi_r w'_\theta) + \alpha^2 w'_\tau \quad (4.33)$$

and

$$\nabla_1^4 \psi + (1/r)(\psi_r \partial/\partial \theta - \psi_\theta \partial/\partial r) \nabla_1^2 \psi = -w' w'_y + \alpha^2 \nabla_1^2 \psi_\tau, \quad (4.34)$$

where  $y = r \sin \theta$ ,  $\tau = \alpha^2 t$  and there is a new dimensionless parameter,  $R_s$ :

$$R_s = \delta W_0^2 / \alpha^2 = \delta \hat{W}_a^2 / \Omega \nu, \quad (4.35)$$

where  $\hat{W}_a$  is the dimensional axial velocity amplitude.  $R_s$  has a large value, of the order of  $10^3$ – $10^4$ , in the aorta. Note that the ratio of the unsteady pressure gradient amplitude to the mean is equal to  $\alpha^3 (2R_s)^{1/2} / D$ . The present notation differs from that of Lyne, Smith and Blennerhassett in that they used  $\beta = \sqrt{2}/\alpha$  instead of  $\alpha$ , and they omitted the  $\sqrt{2}$  from the definitions of  $D$  in (4.9) and of  $w'$ , with the result that the  $w' w'_y$  term in (4.34) was multiplied by 2.

Since the problem has three independent parameters, each of which may be taken to be large or small, there is an enormous variety of different limiting cases for which asymptotic expansions can be sought analytically. Smith (1975) has investigated many of them. Here we restrict attention to those that are potentially of greatest interest in the study of flow in large arteries; that is, we

restrict attention from the start to large values of  $\alpha$ , and to flows in which the amplitude of the oscillatory motion is at least as large as the mean velocity; small perturbations about the steady flow are relatively easy to analyse (Smith, 1975, § 2).

#### 4.2.1 Zero mean pressure gradient

In order to discover the principal effects of oscillations in a curved tube, we follow Lyne (1971) and examine first the case in which the flow is purely oscillatory, i.e.  $D = 0$ . If the fluid were inviscid, there would be potential flow in which

$$w' = \alpha(2R_s)^{1/2} \sin \tau, \quad \psi = 0; \quad (4.36a)$$

this is the dimensionless, small- $\delta$  version of a potential vortex, centred on the centre of curvature of the tube axis, which has dimensional velocity

$$\hat{w} = R\hat{W}_a \sin(\Omega\hat{t})/(R + \hat{r} \cos \theta). \quad (4.36b)$$

In a viscous fluid with large  $\alpha$ , this oscillatory core flow will be surrounded by a Stokes layer on the boundary  $r = 1$ . In that Stokes layer the centrifugal forces will drive an oscillatory secondary motion, primarily consisting of a  $\theta$ -component of velocity,  $v$ . Since the centrifugal force term is proportional to  $w'^2$  (see (4.6) and (4.7)), the solution for  $v$  will contain both an oscillation with double the fundamental frequency, and a mean flow. This mean secondary flow is similar to the steady streaming generated by the high-frequency oscillation of a cylinder or sphere (Riley, 1965); as in those examples, the mean flow does not fall to zero at the edge of the Stokes layer, but drives steady secondary motions in the core. The details of the core flow will depend on the value of the 'secondary-streaming Reynolds number', which in this case is  $R_s$ . This parameter must be allowed to remain  $O(1)$  as  $\alpha \rightarrow \infty$ .

Recognising that a secondary motion will be generated in the core, we seek a solution there of the form

$$w' = \alpha(2R_s)^{1/2} \sin \tau, \\ \psi = \psi_0 + \alpha^{-1}\psi_1 + \alpha^{-2}\psi_2 + O(\alpha^{-3});$$

substitution into (4.34) shows that  $\nabla_1^2\psi_0$  and  $\nabla_1^2\psi_1$  are independent

of  $\tau$ , and that

$$\frac{\partial}{\partial \tau} \nabla_1^2 \psi_2 = \nabla_1^4 \psi_0 + \frac{1}{r} \left( \psi_{0r} \frac{\partial}{\partial \theta} - \psi_{0\theta} \frac{\partial}{\partial r} \right) \nabla_1^2 \psi_0. \quad (4.37)$$

The Stokes layer has a dimensional thickness proportional to  $(\nu/\Omega)^{1/2}$ , so we introduce new variables

$$\eta = (\alpha/\sqrt{2})(1-r), \quad \Psi = \alpha\psi, \quad W = \alpha^{-1}w',$$

and seek solutions of the form

$$W = W_0 + O(\alpha^{-1}), \quad \Psi = \Psi_0 + O(\alpha^{-1}).$$

These must satisfy the no-slip condition on  $\eta = 0$ , and must match to the core flow as  $\eta \rightarrow \infty$ , which among other things requires

$$W_0 \rightarrow (2R_s)^{1/2} \sin \tau \quad \text{as } \eta \rightarrow \infty. \quad (4.38)$$

The equations satisfied by  $W_0$  and  $\Psi_0$ , from (4.33) and (4.34), are

$$\frac{1}{2} W_{0\eta\eta} - W_{0\tau} = -(2R_s)^{1/2} \cos \tau \quad (4.39)$$

and

$$\frac{1}{2} \Psi_{0\eta\eta\eta\eta} - \Psi_{0\eta\eta\tau} = \sqrt{2} \sin \theta W_0 W_{0\eta}. \quad (4.40)$$

The solution of (4.39) satisfying (4.38) and the wall condition is

$$W_0 = (2R_s)^{1/2} [\sin \tau - e^{-\eta} \sin(\tau - \eta)], \quad (4.41)$$

which is the basic Stokes layer solution. This is then substituted into the right-hand side of (4.40); the most general periodic solution that has frequency 2 and satisfies the wall boundary conditions is

$$\begin{aligned} \Psi_0 = & \sqrt{2} R_s \sin \theta \left[ \frac{5}{8} - \frac{1}{4} \eta - \frac{1}{8} e^{-2\eta} - \frac{1}{\sqrt{2}} e^{-\eta} \cos(-\eta + \frac{1}{4}\pi) \right. \\ & + \frac{1}{8\sqrt{2}} (9 - 5\sqrt{2}) \cos(2\tau + \frac{1}{4}\pi) - \frac{1}{8\sqrt{2}} e^{-2\eta} \cos(2\tau - 2\eta + \frac{1}{4}\pi) \\ & \left. - \frac{1}{\sqrt{2}} e^{-\eta} \cos(2\tau - \eta + \frac{1}{4}\pi) + \frac{5}{8} e^{-\sqrt{2}\eta} \cos(2\tau - \sqrt{2}\eta + \frac{1}{4}\pi) \right] \\ & + B(\theta)\eta^3 + C(\theta)\eta^2. \end{aligned} \quad (4.42)$$

As usual in such steady-streaming problems the arbitrary functions  $B(\theta)$  and  $C(\theta)$  turn out on matching to be zero, but not only does  $\Psi_0$  not tend to zero as  $\eta \rightarrow \infty$  (a displacement effect, present in all

boundary layers) but also  $\Psi_{0\eta}$  does not tend to zero as  $\eta \rightarrow \infty$ . In fact, with  $B = C = 0$ ,

$$\begin{aligned}\Psi_0 &\sim \sqrt{2} R_s \sin \theta \left[ \frac{5}{8} - \frac{1}{4} \eta + (1/8\sqrt{2})(9 - 5\sqrt{2}) \cos(2\tau + \frac{1}{4}\pi) \right], \\ \Psi_{0\eta} &\rightarrow -(1/2\sqrt{2}) R_s \sin \theta\end{aligned}\quad (4.43)$$

as  $\eta \rightarrow \infty$ .

The core solution  $\psi_0$  must match with (4.43) as  $r \rightarrow 1$ . Since  $\nabla_1^2 \psi_0$  is independent of  $\tau$ , we can write

$$\psi_0 = \psi_0^{(u)}(r, \theta, \tau) + \psi_0^{(s)}(r, \theta),$$

where  $\psi_0^{(s)}$  is steady and  $\psi_0^{(u)}$  is periodic with zero mean and satisfies  $\nabla_1^2 \psi_0^{(u)} = 0$ . In fact, matching with (4.43) leads to the conclusion that  $\psi_0^{(u)} \equiv 0$ , the unsteady term in (4.43) giving rise only to a displacement effect at higher order in  $\alpha^{-1}$ . Since  $\psi_2$  is expected to contain only periodic and mean terms, (4.37) yields the equation satisfied by  $\psi_0^{(s)}$ :

$$\nabla_1^4 \psi_0^{(s)} + (1/r)(\psi_{0r}^{(s)} \partial/\partial\theta - \psi_{0\theta}^{(s)} \partial/\partial r) \nabla_1^2 \psi_0^{(s)} = 0;$$

and this must be solved subject to the boundary conditions derived from (4.43):

$$\psi_0^{(s)} = 0, \quad \partial\psi_0^{(s)}/\partial r = \frac{1}{4} R_s \sin \theta \quad \text{on } r = 1.$$

If we write  $\psi_0^{(s)} = R_s \chi_0$ ,  $\chi_0$  satisfies

$$\left. \begin{aligned} \frac{1}{R_s} \nabla_1^4 \chi_0 + \frac{1}{r} \left( \chi_{0r} \frac{\partial}{\partial\theta} - \chi_{0\theta} \frac{\partial}{\partial r} \right) \nabla_1^2 \chi_0 &= 0, \\ \chi_0 &= 0, \quad \chi_{0r} = \frac{1}{4} \sin \theta \quad \text{on } r = 1, \end{aligned} \right\} \quad (4.44)$$

which is the problem of the steady, two-dimensional viscous flow in a circle, driven by a given tangential velocity on the boundary. This steady secondary flow in the core is governed by the single dimensionless parameter  $R_s$ , the secondary-streaming Reynolds number.

As usual for viscous flows, analytical progress towards solution of the problem (4.44) can be achieved only in the limits of small and large  $R_s$  (Lyne, 1971). The small- $R_s$  limit is a simple Stokes flow problem, with solution

$$\chi_0 = -\frac{1}{8} r(1-r^2) \sin \theta - (R_s/3072) r^2 (1-r^2)^2 \sin 2\theta + O(R_s^2).$$

Note that  $(1/r)\chi_{0\theta}$ , proportional to the radial velocity, is to leading order *negative* on  $\theta = 0$  (and positive on  $\theta = \pi$ ). This means that the

steady secondary streaming in the core proceeds across the tube from the outside of the bend to the inside. This is in the opposite direction to the secondary flow in a pipe when the axial pressure gradient is steady, and corresponds to the negative value of the azimuthal velocity (proportional to  $-\chi_{0r}$ ) on  $r = 1$ .

At large values of  $R_s$  (more relevant physiologically) one expects the effects of viscosity to be confined to boundary layers of thickness  $R_s^{-1/2}$  near  $r = 1$ ; however, these come together at  $\theta = 0$  and erupt across the centre of the tube. Lyne (1971) postulates (and demonstrates the self-consistency of) a scheme in which the wall boundary layers are supplemented by another layer of thickness  $R_s^{-1/2}$  across the plane of symmetry ( $\theta = 0, \theta = \pi$ ), the bulk of the core flow being inviscid (fig. 4.4). In the inviscid regions the streamlines are closed, and therefore the vorticity is uniform (Batchelor, 1956) and of opposite sign in the two regions; one reason why the shear layer across the middle is required is to smooth out the discontinuity in vorticity between the two inviscid regions. In the upper core region, the stream function (denoted by an overbar) is given by

$$\nabla^2 \bar{\chi}_0 = -\zeta,$$

where  $\zeta$  is the vorticity, expected to be negative (fig. 4.4). The boundary conditions are

$$\bar{\chi}_0 = 0 \quad \text{on } r = 1 \quad \text{and} \quad \text{on } \theta = 0, \pi.$$

The solution is

$$\begin{aligned} \bar{\chi}_0 = \frac{\zeta}{2\pi} \left\{ \left[ 1 - \frac{1}{2} \left( r^2 + \frac{1}{r^2} \right) \cos 2\theta \right] \tan^{-1} \left( \frac{2r \sin \theta}{1 - r^2} \right) \right. \\ \left. - \frac{1}{4} \left( r^2 - \frac{1}{r^2} \right) \sin 2\theta \log \left( \frac{1 + 2r \cos \theta + r^2}{1 - 2r \cos \theta + r^2} \right) \right. \\ \left. + \left( r - \frac{1}{r} \right) \sin \theta - \frac{1}{2} \pi r^2 (1 - \cos 2\theta) \right\}, \end{aligned} \quad (4.45)$$

and this gives the scaled tangential velocity at the edge of the boundary layer on  $r = 1$  to be

$$\bar{v}_1 = -\bar{\chi}_{0r}|_{r=1} = (\zeta/\pi)(\pi \sin^2 \theta - 2 \sin \theta - \sin 2\theta \log \tan \frac{1}{2}\theta),$$

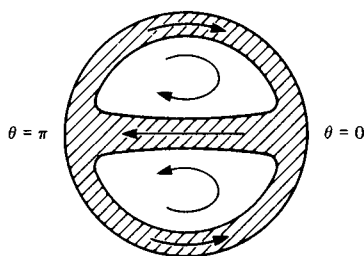


Fig. 4.4. Sketch of cross-section of curved tube showing steady secondary streaming at large values of  $R_s$ . Shaded regions are viscous boundary layers.

while that at the edge of the layer on  $\theta = 0, \pi$  is

$$\bar{u}_1 = \frac{1}{r} \bar{\chi}_{0\theta} |_{\theta=0, \pi} = \frac{\zeta}{2\pi} \left(1 - \frac{1}{x^2}\right) \left[2 - \left(x + \frac{1}{x}\right) \log \left(\frac{1+x}{1-x}\right)\right],$$

where  $x = r \cos \theta$ . The boundary condition to be satisfied by the tangential velocity  $v$  on  $r = 1$  is  $v_0 = -\frac{1}{4} \sin \theta$ . The boundary condition to be satisfied by the tangential velocity  $u$  on  $y = r \sin \theta = 0$  is  $\partial u / \partial y = 0$ ; the value of  $u$  on  $y = 0$  is unknown. The usual two-dimensional boundary layer equations are to be satisfied in each layer. Their exact solution would be a difficult problem, and Lyne (1971) found an approximate solution by assuming (a) that the longitudinal velocity in a shear layer departed by only a little from that in the core just outside, so the equations could be linearised, and (b) that the velocity profile in the shear layers is convected unchanged around the corners at  $\theta = 0, \pi$ . He showed that (b) is self-consistent with the linearisation and with earlier work by Harper (1963) and Moore (1963), but that (a) is inaccurate near  $\theta = 0, \pi$ . This is not expected to be important because the velocities are small there anyway. Lyne's numerical results showed that  $\zeta \approx -0.56$ , and that the secondary flow has stagnation points (the vortex centres) at  $r \approx 0.48$ ,  $\theta = \pm \frac{1}{2}\pi$ . These values should be compared with

$$r \approx 0.58 - 1.04 \times 10^{-6} R_s^2, \quad \theta = \pm \left(\frac{1}{2}\pi - 2.00 \times 10^{-3} R_s\right)$$

when  $R_s$  is small: the vortex centre moves off the line  $\theta = \pm \frac{1}{2}\pi$  in the direction of the fluid motion at  $r = 1$  as  $R_s$  increases from zero, but comes back on to  $\theta = \pm \frac{1}{2}\pi$  as  $R_s \rightarrow \infty$ . Lyne made qualitative

experimental observations of the direction of steady secondary streaming in the core, which was from the outside to the inside of the bend as predicted.

From the physiological point of view, the most important quantities to predict are the axial velocity profile in the core and the wall shear stress. Lyne's theory predicts no departure from a flat profile in the core, because it is limited to infinitesimally small values of  $\delta$ , and the secondary motions affect the profile only at the next order (see § 4.3). The wall shear has two components, which can be calculated from the boundary layer solutions (4.41) and (4.42). In dimensional terms the axial wall shear-rate is

$$\frac{\nu}{a^2} \frac{1}{(2\delta)^{1/2}} \frac{\alpha^2}{\sqrt{2}} W_{0\eta}|_{\eta=0} = \hat{W}_0 \left(\frac{\Omega}{\nu}\right)^{1/2} \sin(\Omega\hat{t} + \tfrac{1}{4}\pi),$$

as in a Stokes layer, and the secondary wall shear-rate is

$$\frac{\nu}{a^2} \frac{1}{2} \alpha \Psi_{0\eta\eta}|_{\eta=0} = \frac{\hat{W}_0^2 \delta}{(\Omega\nu)^{1/2} a} \frac{\sin \theta}{2\sqrt{2}} [1 + (3\sqrt{2} - 5) \sin(2\Omega\hat{t} + \tfrac{1}{4}\pi)].$$

It is interesting to note that the steady component of the secondary shear is in the direction of  $\theta$  increasing (for  $\theta > 0$ ), which is in the opposite sense to the mean velocity at the edge of the Stokes layer, driving the steady streaming in the core.

#### 4.2.2 Non-zero mean pressure gradient

One of the reasons why Lyne's theory is not directly applicable to the aorta is that it requires the mean pressure gradient to be zero. Only if  $D$  is very small (i.e.  $D \ll \alpha^{-1} \ll 1$ ) can the flow be expanded in a power series in  $D$  with Lyne's solution as the leading term (Smith, 1975, § 3). However, in the canine aorta we have  $\alpha \approx 13$ ,  $D \approx 2000$  and  $R_s \approx 4200$ , so although the ratio between the amplitude and the mean of the pressure gradient,  $\alpha^3(2R_s)^{1/2}/D$ , is large (about 100),  $D$  should be taken to be large not small. If the flows associated with the mean and the oscillations could be uncoupled, one would expect the mean to be described by large- $D$  steady flow (§ 4.1.3) and the oscillations by large- $\alpha$ , large- $R_s$  unsteady flow (§ 4.2.1), except that there we let  $\alpha \rightarrow \infty$  before allowing  $R_s \rightarrow \infty$ , while the order of magnitude of the numbers here suggests that the limits should be taken in the reverse order. However, the problem is non-linear and



the mean and oscillatory parts cannot be separated; we should therefore examine carefully those cases in which  $\alpha$ ,  $D$ ,  $R_s$  are all large. The values of the above numbers suggest that we should concentrate particularly on values of the parameters such that  $1 \ll \alpha \ll D < R_s$  (and in which  $D \ll \alpha^3 R_s^{1/2}$ , so that the amplitude of the pressure gradient oscillations is much greater than the mean). The regimes of greatest theoretical interest are those in which the secondary streaming in the core changes from being outwards, as it would be if the pressure gradient were steady and equal to the mean, to being inwards, as if driven by the Stokes layer on the wall in the absence of a mean pressure gradient. *A priori* one would expect this transition to occur when  $R_s = O(D^{1/3})$ , on the assumption that each of the two contributions to the secondary streaming has the same order of magnitude as it would in the absence of the other. However, little work has been done on this case, and the greatest progress in studying such a transition has been made by Blennerhassett (1976) who took the limit  $\alpha \rightarrow \infty$  and then examined cases in which  $D \leq R_s$ . This is physiologically reasonable, apart from the initial limit  $\alpha \rightarrow \infty$ .

Blennerhassett's limiting procedure ensures that the thinnest boundary layer on the tube wall is the Stokes layer, in which the flow is that already calculated by Lyne (1971). Interest can therefore be centred on the steady component of the flow, driven both by the mean axial pressure gradient and by the slip velocity at the edge of the Stokes layer. Blennerhassett showed that if the axial velocity outside the Stokes layer, non-dimensionalised as in the early part of this section, is written

$$w' = \alpha(2R_s)^{1/2} \sin \tau + w_1 + O(\alpha^{-1}),$$

and if the stream function is again written as

$$\psi = \psi_0 + \alpha^{-1} \psi_1 + O(\alpha^{-2}),$$

then the equations for  $w_1$  and  $\psi_0$  are just the equations for exactly steady flow in a curved tube, (4.11) and (4.12), with  $(w', \psi)$  replaced by  $(w_1, \psi_0)$ . The boundary conditions, however, are different from those in § 4.1, being

$$\psi_0 = w_1 = 0, \quad \psi_{0r} = \frac{1}{4}R_s \sin \theta \quad \text{on } r = 1. \quad (4.46)$$

The solution of this problem in the limit  $R_s \rightarrow \infty$  with  $D = o(R_s)$  reveals that the secondary stream function  $\psi_0 (= O(R_s))$  becomes equal to that calculated by Lyne (1971), so that the flow in the core (away from the steady-streaming boundary layer) is given by  $\psi_0 = R_s \bar{\chi}_0$  and (4.45) above. The axial velocity  $w_1$  is then to be calculated from (4.11). This equation suggests that  $w_1 = O(D/R_s)$ , so that in the core the axial flow results from a balance between the convective and the pressure gradient terms. However, by converting to (secondary) streamline coordinates, Blennerhassett was able to show that such a balance leads to a solution for  $w_1$  that is not a single-valued function of position, and hence  $w_1$  must be  $O(D)$ . Thus  $w_1$  in the core must satisfy

$$\bar{\chi}_{0\theta} w_{1r} - \bar{\chi}_{0r} w_{1\theta} = 0,$$

which means that  $w_1$  is constant on the secondary streamlines. In fact, examination of the equations for the  $O(DR_s^{-1/2})$  and  $O(DR_s^{-1})$  corrections to  $\bar{\chi}_0$  shows that

$$w_1(r, \theta) = (D/\zeta) \bar{\chi}_0(r, \theta)$$

in the core, where  $\zeta (\approx 0.56)$  is the magnitude of the axial vorticity in each of the two inviscid core regions, separated by a shear layer across the middle of the tube (fig. 4.4). In this limit, therefore, the secondary flow is inwards across the core, as in purely oscillating flow, and there are peaks of axial velocity at the vortex centres in each half of the tube. Blennerhassett also gave an approximate numerical solution of the equations for  $w_1$  in the wall and centre-plane boundary layers (thickness  $\propto R_s^{-1/2}$ ) using Lyne's solution for  $\psi_0$ .

More important than these asymptotic results, however, are Blennerhassett's numerical solutions for the steady components of the flow, obtained directly from (4.11) and (4.12) for arbitrary values of  $D$  and  $R_s$ , without any boundary layer approximation. He first solved the equations for  $D = o(R_s)$ , in which case the secondary stream function is not affected by the axial flow and is determined from (4.44) as in the purely oscillatory case. Then  $w_1$  is given by solving the linear equations (4.11). Results for various values of  $R_s$  are shown in fig. 4.5. In each part of the figure the secondary streamlines are shown on the left, and contours of axial velocity on

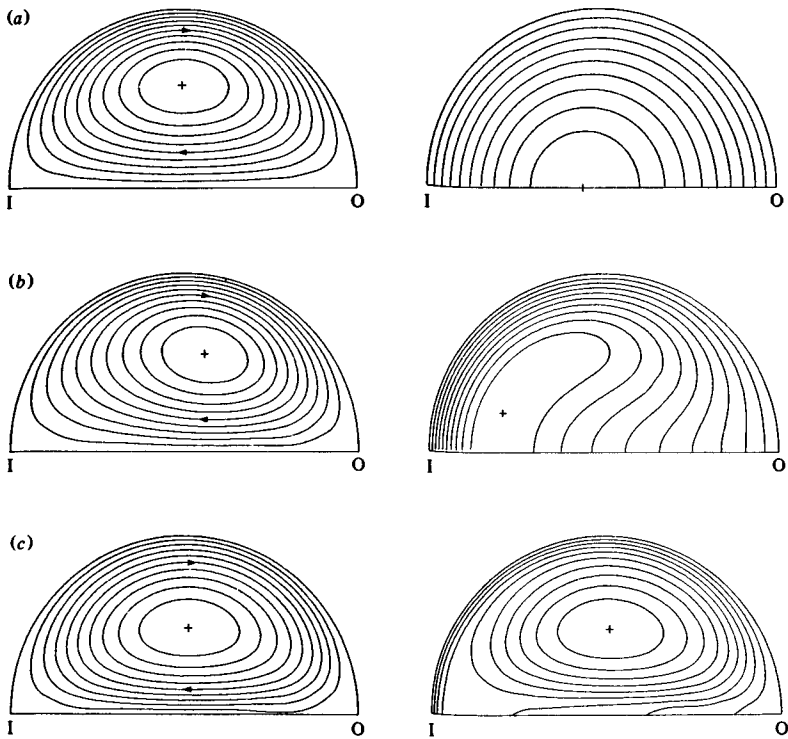


Fig. 4.5. Plots of secondary streamlines (left) and of axial velocity contours (right) representing the steady flow induced by pulsatile motion in a curved tube. I is the inside of the bend, O the outside. Here  $D = o(R_s)$ , (a)  $R_s = 10$ , (b)  $R_s = 150$ , (c)  $R_s = 1800$ . (After Blennerhassett, 1976.)

the right. The secondary streamlines show no qualitative changes with  $R_s$ , the velocity being inwards across the centre of the tube, but the axial velocity distribution changes considerably. At fairly small  $R_s$  (e.g.  $R_s = 10$ , fig. 4.5(a)) the axial velocity represents only a small deviation from axial symmetry (Poiseuille flow). As  $R_s$  is increased, however, axial momentum is advected towards the inside wall of the bend, and is swept round sideways, so that the peak axial velocity occurs much closer to the inside wall. Furthermore, at a value of  $R_s$  between 100 and 150, the position of peak axial velocity comes off the centre plane (fig. 4.5(b), for  $R_s = 150$ ), and, as  $R_s \rightarrow \infty$ , this position tends to coincide with the secondary vortex centre (fig. 4.5(c), for  $R_s = 1800$ ). These calculations confirm the asymptotic

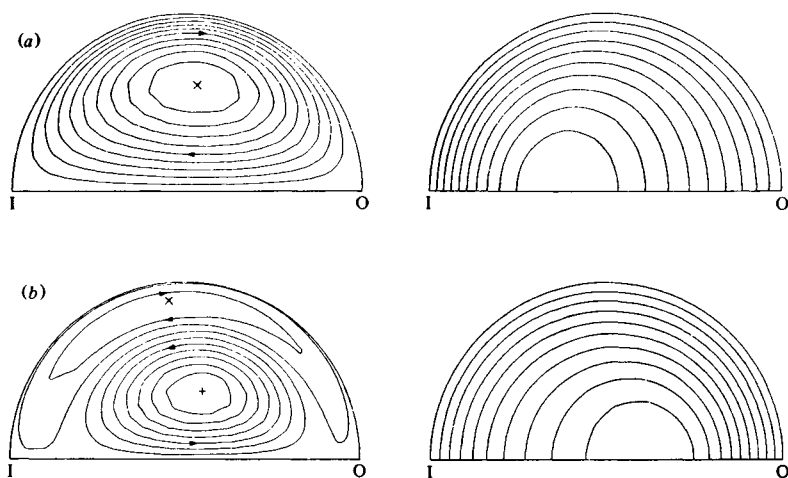


Fig. 4.6. Plots of secondary streamlines (left) and of axial velocity contours (right) representing the steady flow induced by pulsatile motion in a curved tube. I is the inside of the bend, O the outside. Here  $R_s = 30$ , (a)  $D = 40$ , (b)  $D = 160$ . (After Blennerhassett, 1976.)

result that the contours of constant  $w_1$  coincide with the secondary streamlines when  $R_s \rightarrow \infty$ .

When  $D$  is not much smaller than  $R_s$ , (4.11) and (4.12) are not uncoupled, and must be solved simultaneously. Their solution yields some very interesting results. At fairly small values of  $R_s$  they are not unexpected, as shown by fig. 4.6 for  $R_s = 30$ , and (a)  $D = 40$ , (b)  $D = 160$  (the Dean number defined by (4.9) and used here is eight times that used by Blennerhassett). When  $D$  is small, the secondary streaming is directed towards the inside wall (fig. 4.6(a)), and the peak axial velocity occurs near the inside wall. As  $D$  is increased, however, the influence of the steady axial pressure gradient becomes stronger, and the secondary flow driven by the slip velocity at the edge of the Stokes layer is squeezed to the sides, to be replaced in the core by a secondary flow directed outwards, as in steady flow (fig. 4.6(b)). The peak axial velocity then moves towards the outside of the tube. This sequence of solutions is consistent with that predicted by Blennerhassett for creeping flow ( $R_s \ll 1$ ).

For somewhat larger values of  $R_s$ , the transition from inwards to outwards secondary flow continues to arise in much the same way.

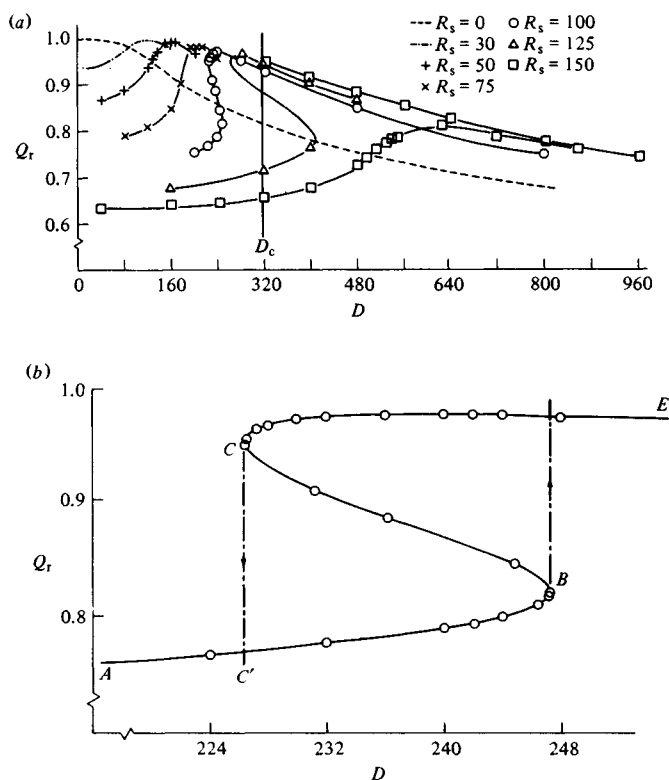


Fig. 4.7. (a) Plots of the flow-rate ratio,  $Q_r$ , against  $D$ , for various values of  $R_s$ .  $Q_r$  is the actual flow-rate through the tube at a given mean pressure gradient divided by the flow-rate in a straight tube driven by the same mean pressure gradient. (b) Enlargement of the S-shaped section of the curve for  $R_s = 100$ . (After Blennerhassett, 1976.)

However, for values of  $R_s$  above a certain critical value, between 75 and 100, a most unexpected result is obtained. This is best exhibited in graphs of mean volume flow-rate through the tube, expressed as a fraction of the mean flow-rate in a straight tube with the same mean pressure gradient, against  $D$  for various values of  $R_s$ . Fig. 4.7(a) shows that for  $R_s$  below its critical value the flow-rate ratio,  $Q_r$ , is a single-valued function of  $D$  with a maximum at a value of  $D$  that is predicted to be approximately  $22R_s^{1/2}$  when  $R_s$  is small. This value is slightly above that at which the transition in the nature of the secondary flow takes place.

For  $R_s$  equal to 100 or more, however, an S-shaped portion appears in the graph of  $Q_r$  against  $D$ , with the implication that the value of  $Q_r$  actually achieved at a given  $D$  depends on how the flow is started. If  $D$  is gradually increased from zero, with  $R_s$  fixed, the flow-rate will follow the lower branch of the curve, jumping discontinuously to the upper branch when  $D$  reaches the value at which the slope of the curve becomes infinite (point  $B$  on fig. 4.7(b)). Similarly, if  $D$  is reduced from a very large value,  $Q_r$  will follow the upper branch, jumping discontinuously to the lower branch at the point  $C$ . Blennerhassett was able to compute flow patterns corresponding to points on each section of the curve. He found that the flows do represent a one-parameter family of solutions of the equations, with the axial velocity on the centre line increasing monotonically as the curve is followed continuously from point  $A$  to point  $E$  (fig. 4.7(b)). Some of his computations are also shown in fig. 4.8, and confirm that the steady secondary flow corresponding to points on the lower branch of the curve has the same direction as for a purely oscillatory pressure gradient (fig. 4.8(a)), while for points on the upper branch the secondary flow in the core resembles that for a steady pressure gradient (fig. 4.8(c) and (d)). The middle branch represents an intermediate type of flow (fig. 4.8(b)), but this is presumably unstable and unrealisable in practice.

Even more unexpected results were obtained for  $R_s = 150$  (the largest value considered by Blennerhassett). Here it seems as if the point  $B$  of fig. 4.7(b) has gone off to infinity, and at least two solutions of the problem exist for all  $D$  above  $D_c$  (fig. 4.7(a)). In this case the flow on the upper branch would be achieved only if a secondary motion with outwards velocity on the centre plane were imposed at the start (i.e. if  $R_s$  were increased from zero with  $D$  fixed), and that on the lower branch only if an inwards secondary motion were imposed at the start (or if  $D$  were gradually increased from zero). The flow patterns corresponding to the lower branch have features in common with the large- $R_s$ ,  $D = O(R_s)$  results, in that the positions of maximum axial velocity do not lie on the centre plane (compare fig. 4.9 with figs. 4.5(b), (c)). The upper-branch flow patterns are qualitatively the same as other upper-branch patterns, such as that shown in fig. 4.8(d).

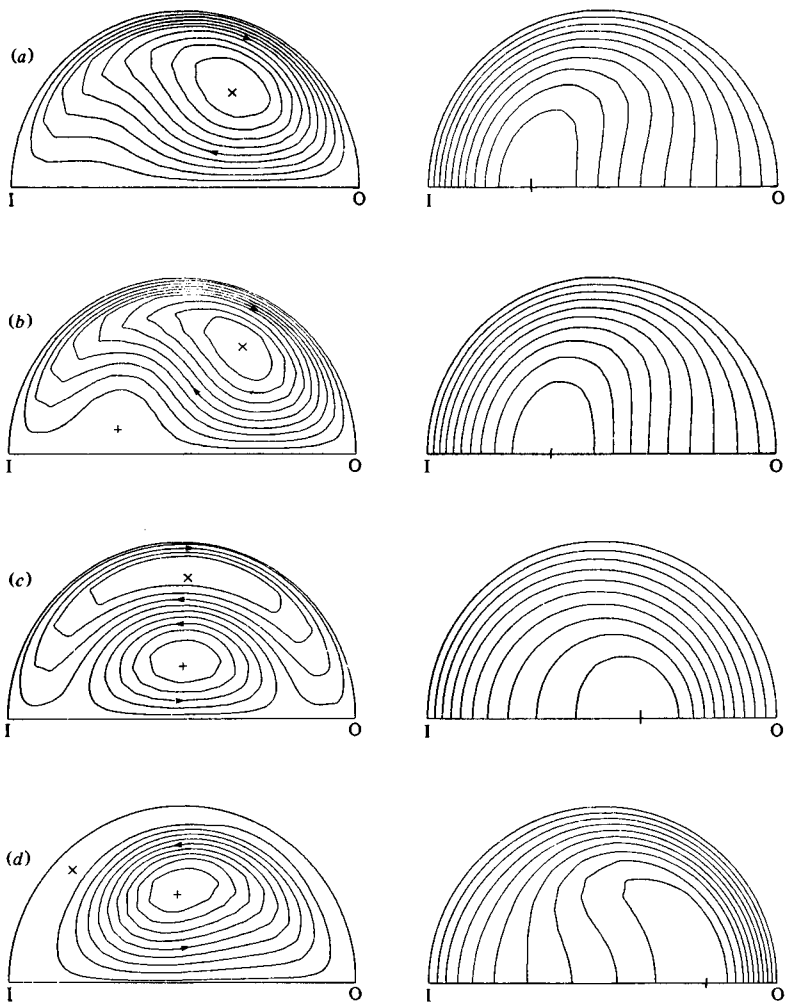


Fig. 4.8. Plots of secondary streamlines (left) and of axial velocity contours (right) representing the steady flow induced by pulsatile motion in a curved tube. I is the inside of the bend, O the outside. Here  $R_s = 100$ , (a)  $D = 244$  (lower branch of curve in fig. 4.7(b)), (b)  $D = 245$  (middle branch), (c)  $D = 244$  (upper branch), (d)  $D = 400$ . (After Blennerhassett, 1976.)

These results are too novel and too incomplete for a genuine physical or mathematical understanding to be available as yet. It is clear both that (4.11) and (4.12), with boundary conditions (4.46),

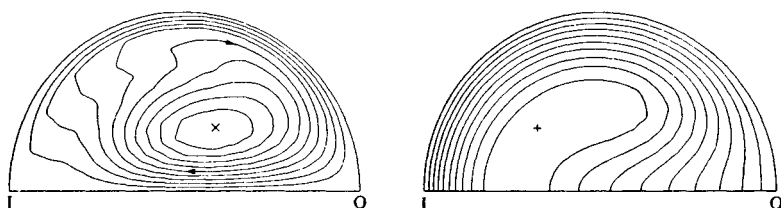


Fig. 4.9. Plots of secondary streamlines (left) and of axial velocity contours (right) representing the steady flow induced by pulsatile motion in a curved tube. I is the inside of the bend, O the outside. Here  $R_s = 150$ ,  $D = 512$  (lower branch of curve in fig. 4.7(b)). (After Blennerhassett, 1976.)

contain a wealth of fascinating information and that the problem of pulsatile flow in a curved tube is far from completely solved, even in the limit  $\alpha \rightarrow \infty$ .

Returning now to cases in which the Stokes layer is not necessarily the thinnest layer present, i.e. the limit  $\alpha \rightarrow \infty$  is not taken before any other, we recall that the thickness of the boundary layer in steady flow at large  $D$  is  $O(D^{-1/3})$ , while the Stokes layer has thickness  $O(\alpha^{-1})$ . Thus important interactions in the boundary layer can be expected when  $\alpha = O(D^{1/3})$ , and again the numbers quoted on p. 183 suggest that this is a physiologically important regime ( $2000^{1/3} \approx 12.6$ ). As in § 4.1.3, let  $w' = D^{2/3} \tilde{w}$ ,  $\psi = D^{1/3} \tilde{\psi}$  and also set  $\alpha = \tilde{\alpha} D^{1/3}$ . Then in the inviscid core, the equations of motion are

$$\left. \begin{aligned} D^{1/3} \tilde{\alpha}^2 \tilde{w}_\tau + (1/r)(\tilde{\psi}_\theta \tilde{w}_r - \tilde{\psi}_r \tilde{w}_\theta) &= \tilde{\alpha}^3 (2R_s)^{1/2} \cos \tau + 1, \\ D^{-1/3} \tilde{\alpha}^2 \nabla_1^2 \tilde{\psi}_\tau - \tilde{w} \tilde{w}_y &= (D^{-2/3}/r)(\tilde{\psi}_r \partial/\partial \theta - \tilde{\psi}_\theta \partial/\partial r) \nabla_1^2 \tilde{\psi}, \end{aligned} \right\} \quad (4.47)$$

where  $y = r \sin \theta$ . In the boundary layer, we make the substitution  $\zeta = D^{1/3}(1-r)$  and obtain to leading order (cf. (4.25) and (4.26a))

$$\left. \begin{aligned} -\tilde{\alpha}^2 \tilde{w}_\tau + \tilde{w}_{\zeta\zeta} + \tilde{\psi}_\theta \tilde{w}_\zeta - \tilde{\psi}_\zeta \tilde{w}_\theta &= -\tilde{\alpha}^3 D^{-1/3} (2R_s)^{1/2} \cos \tau, \\ -\tilde{\alpha}^2 \tilde{\psi}_{\zeta\zeta\tau} + \tilde{\psi}_{\zeta\zeta\zeta} + \tilde{\psi}_\theta \tilde{\psi}_{\zeta\zeta} - \tilde{\psi}_\zeta \tilde{\psi}_{\zeta\theta} &= \sin \theta \tilde{w} \tilde{w}_\zeta. \end{aligned} \right\} \quad (4.48)$$

In order that the unsteady terms in (4.48) should formally be of the same order of magnitude as the others, we set  $(2R_s)^{1/2} = S D^{1/3}$ , although we recognise that  $S$  must be allowed subsequently to be large.

The second of equations (4.47) shows that the leading term in the expansion for the axial velocity in the core represents a



non-interacting combination of the steady and the unsteady motion. The expansion can therefore be written

$$\tilde{w} = \tilde{\alpha} S \sin \tau + w_{c0}(x) + D^{-1/3} w_{c1}(x, y, \tau) + O(D^{-2/3}),$$

where  $x = r \cos \theta$ . The leading term in the stream function expansion, however, cannot be uncoupled from the unknown function  $w_{c1}$ ; equations (4.47) yield (Smith, 1975, § 8):

$$\tilde{\psi} = \tilde{\psi}_0 + O(D^{-1/3}),$$

where

$$\tilde{\psi}_0 = \left[ y - \tilde{\alpha}^2 \int_0^y w_{c1,\tau} dy \right] / w'_{c0}(x),$$

$$\frac{\partial}{\partial \tau} (\nabla_1^2 \tilde{\psi}_0) = \frac{(\tilde{\alpha} S \sin \tau + w_{c0})}{\tilde{\alpha}^2} w_{c1,y}.$$

Furthermore, the boundary layer equations (4.48) are intrinsically unsteady, and not even in the axial velocity can the steady and unsteady components of the flow be uncoupled. Smith (1975, § 6) was able to make some progress in the case  $S \ll 1$ , for then the leading steady term is the large- $D$  steady solution, which interacts with the unsteadiness in a modified Stokes layer for which he derived the equations, but did not give a solution. For large  $S$ , however, even he made no progress, because the 'steady-streaming boundary layer' is predicted to be much thinner than the Stokes layer, so that Lyne's sequence of embedded boundary layers cannot describe the flow.

In summary, the situation for oscillatory flows in curved tubes, even when  $\delta \ll 1$ , is unsatisfactory, because although the purely oscillatory case is well understood, and although many cases with a mean pressure gradient have been analysed by Smith (1975) and by Blennerhassett (1976), the case of most physiological relevance is not apparently susceptible to asymptotic analysis, and has not yet received the necessary numerical treatment.

### 4.3 Fully developed unsteady flow starting from rest

Even if a solution were available for the case of sinusoidally oscillating flow in a curved tube with non-zero mean, at values of the parameters  $\alpha$ ,  $D$ ,  $R_s$  pertinent to the aorta, it would not be directly

applicable physiologically, because all the above expansions take the limit  $\delta \rightarrow 0$  before any other limit, whereas in fact  $\delta$  ( $\approx 0.2$ ) is rather greater than any other relevant small parameter ( $\alpha^{-1}$ ,  $D^{-1/3}$ ,  $R_s^{-1/2}$ , etc.). Furthermore, the pulse is not sinusoidal, and, in the intrinsically non-linear circumstances that obtain, the flow resulting from a realistic pressure gradient waveform is likely to be quite different from those already described. We have seen in § 3.2 that it is reasonable to assume that the flow in the aorta starts from rest each beat. In this section, therefore, we examine fully developed flow in a curved tube on this assumption, and hope that the results, expressed in powers of  $t$ , can be used in § 4.4 to describe the purely diffusive downstream flow to which unsteady entry flow must match. We also do not require the assumption  $\delta \ll 1$ , although the time for which the proposed solution is valid will be longer for smaller values of  $\delta$ . The effects of slowly varying curvature can also be included in the expansion. If the curvature is non-uniform, the secondary motions cannot be represented by a stream function, and it is necessary to go back to the original governing equations, (4.1)–(4.4). Working from these equations also makes it easier to give a physical interpretation of the expansion; we therefore use them even for uniform  $\delta$ . We also choose an axial velocity scale,  $\hat{W}_0$ , that is representative of the peak core velocity (not of viscous diffusion), so the Reynolds number,  $Re$ , is not equal to 1; we take it to be large.

#### 4.3.1 Uniform curvature

We suppose that the flow is started at  $t = 0$  in such a way that the dimensionless axial velocity on the centre line,  $W_0(t)$ , varies with time in a given way, such as that shown in fig. 3.3. In fact, we shall for simplicity make calculations using a crude polynomial representation of the physiological waveform, given by

$$\begin{aligned} W_0(t) &= (4t/t_1)(1 - t/t_1) & \text{for } 0 \leq t \leq t_1 \\ &= 0 & \text{for } t_1 \leq t \leq t_2, \end{aligned} \quad (4.49)$$

which has a maximum value of 1 at  $t = \frac{1}{2}t_1$  (fig. 4.10). To correspond with the aortic waveform,  $t_2$  would be approximately equal to  $\hat{W}_0 \hat{T}/a$ , where  $\hat{W}_0$  is the peak axial velocity,  $\hat{T}$  is the period of the

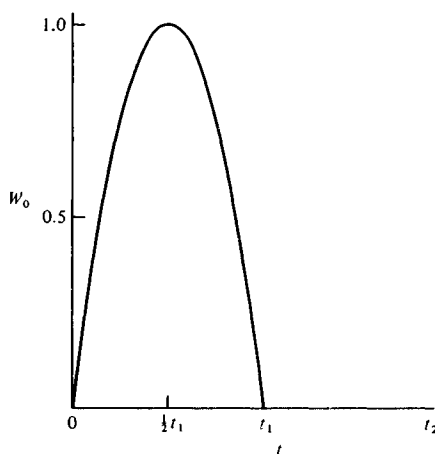


Fig. 4.10. Sketch of centre-line velocity waveform given by (4.49).

beat and  $a$  is the radius of the aorta; in a dog the values given in table 1.1 suggest that  $t_2 \approx 80$ , while  $t_1$  is about a third of this value.

The sequence of events is then as follows: initially the flow everywhere except at the wall will be irrotational, so that the velocity field (for constant curvature) is

$$(u, v, w) = [0, 0, W_0(t)/h], \quad (4.50)$$

and the corresponding pressure field is

$$p_0(r, \theta, s, t) = -s\dot{W}_0(t) - (1/2h^2)W_0^2(t), \quad (4.51)$$

where

$$h = 1 + \delta r \cos \theta. \quad (4.52)$$

Vorticity will immediately begin to diffuse out from the wall, and for a short time the flow can be described in the same way as in a Rayleigh layer, with the only vorticity being azimuthal and occupying a layer of thickness proportional to  $(t/Re)^{1/2}$  (cf. (3.33)). In the Rayleigh layer, however, the velocity is less than  $W_0/h$ , while the pressure is still given by (4.51), and there is a pressure gradient directed from the outside of the bend towards the inside. This will drive a secondary motion in the boundary layer, from outside to inside, which will erupt back into the core at the inside wall. Initially, the axial wall shear is smaller at the outside of the bend,

because  $W_0/h$  is smaller there and the boundary layer is of uniform thickness. However, the convective effect of the secondary motion will be to make the boundary layer thinner at the outside of the bend and thicker at the inside, so that the axial wall shear at the inside will decrease more rapidly than that at the outside, and after a time the shear at the outside will exceed that at the inside as in steady flow (§ 4.1). A separate effect will be the acceleration of the core flow because of the growing displacement thickness of the boundary layer. All these effects will continue throughout the cycle, although after  $t_1$  (fig. 4.10), the forcing by  $W_0(t)$  disappears, and the motion gradually diffuses away to rest. In this section we analyse the flow by representing the velocity components as power series in  $t$ , recognising that the validity of the solution will be restricted to times less than that at which higher-order terms in the expansion became as great as lower-order terms. The analysis will be developed for the case of constant curvature, and the corrections required to account for slowly varying curvature will be described afterwards.

We shall restrict attention to dimensional times short compared with the viscous diffusion time  $a^2/\nu$ , because this is several times greater than the length of one cycle; in dimensionless terms this means that  $t = O(1) \ll Re$ . We expect that vorticity will at all times be restricted to a boundary layer of thickness proportional to  $(t/Re)^{1/2}$ , and therefore introduce new variables

$$\eta = (1-r)(Re/4t)^{1/2}, \quad u' = Re^{1/2}u, \\ w' = w - W_0/h, \quad p' = p - p_0,$$

the other variables remaining unchanged. The governing equations, (4.1)–(4.4), with  $d\delta/ds = 0$ , now become, to leading order in  $Re^{-1/2}$ ,

$$-\frac{1}{(4t)^{1/2}}u'_n + v_\theta - v\frac{\delta \sin \theta}{h} = 0, \quad (4.53)$$

$$p'_\eta = 0 \quad (\text{whence } p' \equiv 0), \quad (4.54)$$

$$v_t - \frac{\eta}{2t}v_n - \frac{u'}{(4t)^{1/2}}v_n + vv_\theta + \frac{\delta \sin \theta}{h}\left(\frac{2W_0w'}{h} + w'^2\right) = -p'_\theta + \frac{1}{4t}v_{\eta\eta}, \quad (4.55)$$

$$w'_t - \frac{\eta}{2t} w'_\eta - \frac{u'}{(4t)^{1/2}} w'_\eta + v \left( w'_\theta - w' \frac{\delta \sin \theta}{h} \right) = -\frac{1}{h} p'_s + \frac{1}{4t} w'_{\eta\eta}. \quad (4.56)$$

In all three equations  $h = 1 + \delta \cos \theta$ , and we have used the fact that  $(\partial/\partial\theta)(1/h) = (\delta \sin \theta)/h^2$ . The next order in  $Re^{-1/2}$  would have to be included to account for the displacement effect; as in § 3.2, however, we ignore it. The boundary conditions are

$$u' = v = 0, \quad w' = -W_0/h \quad \text{on } \eta = 0, \\ v, w' \rightarrow 0 \quad \text{as } \eta \rightarrow \infty.$$

The Rayleigh layer that forms immediately is described by (4.56) with  $v = u' = p'_s = 0$ . The solution is

$$w' = -\frac{1}{h} \frac{2}{\sqrt{\pi}} \int_\eta^\infty W_0 \left( t - \frac{t\eta^2}{\mu^2} \right) e^{-\mu^2} d\mu, \quad (4.57a)$$

or, for the particular form (4.49) of  $W_0(t)$ ,

$$w' = -\frac{1}{h} \left\{ \frac{4t}{t_1} \left[ \operatorname{erfc} \eta (1 + 2\eta^2) - \frac{2}{\sqrt{\pi}} \eta e^{-\eta^2} \right] \right. \\ \left. + \frac{4t^2}{t_1^2} \left[ \operatorname{erfc} \eta (-1 - 4\eta^2 - \frac{4}{3}\eta^4) + \frac{2}{3\sqrt{\pi}} \eta e^{-\eta^2} (5 + 2\eta^2) \right] \right\} \quad (4.57b)$$

when  $t < t_1$ . As  $t \rightarrow 0$ , this solution and  $W_0$  are  $O(t)$ , so that the secondary velocity  $v$  is  $O(t^3)$  from (4.55), and the normal velocity  $u'$  must be  $O(t^{7/2})$  for consistency. The effect of the secondary motion on the axial velocity profile is described by (4.56), which shows that the error in  $w'$  is  $O(t^5)$ , so that both terms of (4.57b) are correct. Even if we had chosen a quartic function to describe  $W_0(t)$ , as did Farthing (1977) in order to model the physiological waveform more closely, the quartic series derived from (4.57a) would have been valid, since the first correction is  $O(t^5)$ .

If we write

$$v = t^3 \sum_{n=0}^{\infty} t^n v_n(\eta, \theta), \\ u' = t^{7/2} \sum_{n=0}^{\infty} t^n u'_n(\eta, \theta), \\ w' = \frac{1}{h} t \sum_{n=0}^{\infty} t^n w'_n(\eta, \theta),$$

where  $w'_0$  and  $w'_1$  are independent of  $\theta$  and are defined by (4.57b), and  $w'_2 = w'_3 = 0$ , we can obtain successively all the unknown functions. For example, the equation satisfied by  $v_0$  is

$$v_{0\eta\eta} + 2\eta v_{0\eta} - 12v_0 = \frac{4\delta \sin \theta}{h^3} w'_0 (w'_0 + 8/t_1), \quad (4.58)$$

which has to be solved subject to the boundary conditions  $v_0 = 0$  at  $\eta = 0$  and as  $\eta \rightarrow \infty$ . This is most easily done numerically, and the solution has been computed by Farthing (1977), who obtained

$$v_{0\eta}|_{\eta=0} = \frac{13.9}{t_1^2} \frac{\delta \sin \theta}{h^3}$$

(needed for the leading term of the secondary wall shear). Similarly, the normal velocity  $u'_0$  satisfies

$$u'_{0\eta} = 2 \left( v_{0\theta} - \frac{\delta \sin \theta}{h} v_0 \right),$$

and this can be integrated, subject only to  $u' = 0$  at  $\eta = 0$ . As  $\eta \rightarrow \infty$ ,

$$u'_0 \rightarrow \frac{3.04}{t_1^2} \left( \frac{\delta \cos \theta}{h^3} + \frac{2\delta^2 \sin^2 \theta}{h^4} \right),$$

which gives rise in the core to the first displacement effect at  $O(Re^{-1/2} t^{7/2})$ . The equation for the first correction,  $w'_4$ , to  $hw'$  is

$$w'_{4\eta\eta} + 2\eta w'_{4\eta} - 20w'_4 = -2u'_0 w'_{0\eta}, \quad (4.59)$$

and this must be solved subject to the same boundary conditions as (4.58). Farthing has also solved this equation, as well as those corresponding to several higher powers of  $t$ . His results for the two components of dimensionless wall shear stress are

$$\begin{aligned} \left( \frac{Re}{4t} \right)^{1/2} w'_\eta|_{\eta=0} &= \left( \frac{Re}{4t} \right)^{1/2} \left\{ \frac{16t}{ht_1\sqrt{\pi}} \left( 1 - \frac{4t}{3t_1} \right) \right. \\ &\quad + \frac{t^5}{t_1^3 h^4} \left( \delta \cos \theta + \frac{2\delta^2 \sin^2 \theta}{h} \right) \\ &\quad \left. \times \left( 0.962 - 2.18 \frac{t}{t_1} \right) + O(t^7) \right\}, \quad (4.60) \end{aligned}$$

$$\left( \frac{Re}{4t} \right)^{1/2} v_\eta|_{\eta=0} = \left( \frac{Re}{4t} \right)^{1/2} \left[ \frac{t^3}{t_1^2} \frac{\delta \sin \theta}{h^3} \left( 13.9 - 24.4 \frac{t}{t_1} \right) + O(t^5) \right]. \quad (4.61)$$

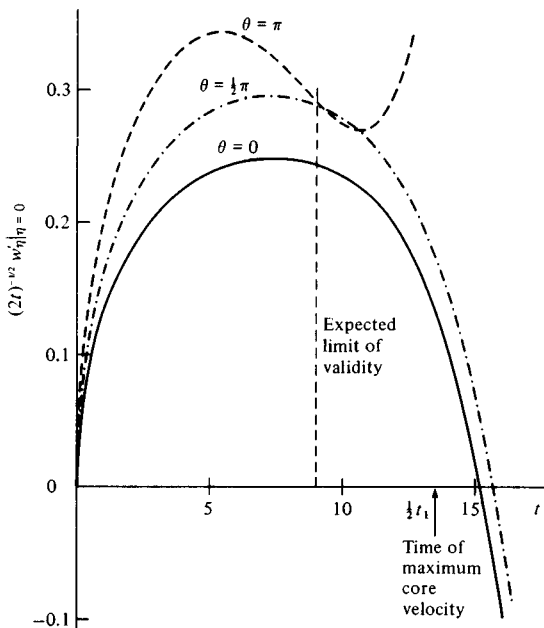


Fig. 4.11. Dimensionless wall shear ( $\times Re^{-1/2}$ ) on the outside ( $\theta = 0$ ), side ( $\theta = \frac{1}{2}\pi$ ) and inside ( $\theta = \pi$ ) walls as a function of  $t$ , calculated from (4.60) with  $\delta = 0.2$ ,  $t_1 = 27$ . The theory is not expected to be accurate for  $t \geq 9.0$ .

Equation (4.60), evaluated at  $\theta = 0$ ,  $\theta = \frac{1}{2}\pi$  and  $\theta = \pi$ , is plotted against  $t$  in fig. 4.11, for  $\delta = 0.2$ ,  $t_1 = 27$ , values appropriate to the aorta. As expected, the shear on the inner wall ( $\theta = \pi$ , so  $h = 1 - \delta$ ) is initially greater than that on the outer wall ( $h = 1 + \delta$ ), but it reaches its maximum value earlier and starts to fall rapidly; the shear on the side-wall ( $\theta = \frac{1}{2}\pi$ ) is intermediate between the two. The shear everywhere reaches a peak long before the time of peak core velocity,  $t = \frac{1}{2}t_1$ . The shear on the inner wall is not predicted to reverse before that on the outer wall (despite our physical expectations) because this series solution becomes invalid before that would occur. This may be assessed by, for example, calculating the time at which  $t^5 \delta \cos \theta / t_1^3 h^4$  is equal to about 0.4 times  $16t/t_1 h \sqrt{\pi}$  (see (4.60)) at  $\theta = \pi$ , when  $h$  is smallest; the critical value of  $t$  is about 9.0 ( $= \frac{1}{3}t_1$ ). Thereafter one might expect that subsequent, neglected terms in the series become as big as those retained. This time,  $t = 9.0$ , which is also approximately the time at which the

shear on the inner wall falls as low as that on the side-walls (fig. 4.11), corresponds in a dog's aorta to about 0.056 s after the beginning of systole. We may notice, however, that the series for  $w'$  and  $v$  are effectively power series in  $\delta t^3$ , so that they remain valid for a longer time as  $\delta$  is reduced.

In addition to computing the above expansions, Farthing has performed a direct finite-difference integration of the boundary layer equations, (4.53)–(4.56). His computations confirm the series solutions exactly for sufficiently small  $t$ , and the numerical solutions also break down near  $\theta = \pi$  shortly before peak systole ( $t = \frac{1}{2}t_1$ ). This breakdown is associated with a marked thickening of the boundary layer at the inside wall ( $\theta = \pi$ ), which is where the secondary motions begin to encroach on the previously undisturbed core flow. From that time on, the core flow will be increasingly modified and the present expansion cannot represent it. However, it gives a good description of the initial generation and modification of the secondary flow.

#### 4.3.2 *Slowly varying curvature*

The above expansion can be extended to cover the case where  $\delta$  varies with  $s$  over a dimensionless length-scale  $1/\varepsilon \gg 1$ ; we can write  $\delta \equiv \delta(\varepsilon s)$ . The irrotational core flow is altered, because if the velocity field is given by (4.50), (4.1) is not satisfied to  $O(\varepsilon)$  when  $h$  depends on  $\varepsilon s$ . Therefore the core flow is given by

$$(u, v, w) = [0, 0, W_0(t)/h] + \varepsilon \delta'(\varepsilon s) W_0(t) \nabla \phi_1 + O(\varepsilon^2) \quad (4.62)$$

and the pressure by

$$p = p_0 + \varepsilon \delta'(\varepsilon s) p_1 + O(\varepsilon^2). \quad (4.63)$$

The perturbation velocity potential  $\phi_1$  is given by

$$\nabla^2 \phi_1 = r \cos \theta / h^3, \quad \phi_{1,r} = 0 \quad \text{on } r = 1$$

where

$$\nabla^2 \phi_1 = \phi_{1,rr} + \frac{1}{r} \phi_{1,r} + \frac{1}{r^2} \phi_{1,\theta\theta} + \frac{\delta \cos \theta}{h} \phi_{1,r} - \frac{\delta \sin \theta}{rh} \phi_{1,\theta} + \frac{1}{h^2} \phi_{1,ss},$$



together with an integral constraint representing the condition that the volume flux along the tube is uniform. The integral constraint states that

$$W_0(t) \int_0^{2\pi} \int_0^1 \left( \frac{1}{h} + \frac{\varepsilon \delta'(\varepsilon s)}{h} \phi_{1s} \right) r \, dr \, d\theta$$

should be independent of  $s$ . Now

$$h = 1 + \delta(\varepsilon s)r \cos \theta \approx 1 + \delta(0)r \cos \theta + \varepsilon s \delta'(0)r \cos \theta + O(\varepsilon^2)$$

as long as  $s = O(1)$ : this implies a particular choice of  $s = 0$ . Hence the integral constraint becomes, approximately,

$$\int_0^{2\pi} \int_0^1 \frac{\phi_{1s}}{1 + \delta_0 r \cos \theta} r \, dr \, d\theta = \int_0^{2\pi} \int_0^1 \frac{s r \cos \theta}{(1 + \delta_0 r \cos \theta)^2} r \, dr \, d\theta, \quad (4.64)$$

where  $\delta_0 = \delta(0)$ . It is clear from the formulation of this problem that it can be solved in the form

$$\phi_1 = \frac{1}{2} \kappa s^2 + \phi_2(r, \theta), \quad \kappa = \text{constant}, \quad (4.65a)$$

and (4.64) shows that

$$\kappa = (1/\delta_0)[1 - (1 - \delta_0^2)^{-1/2}] < 0. \quad (4.66)$$

However, the explicit solution for  $\phi_2$  can apparently be derived only as a power series in  $\delta_0$ . The first two terms in  $\phi_1$  are

$$\phi_1 = \frac{1}{8}(r^3 - 3r) \cos \theta + \delta_0 \left[ -\frac{1}{4}s^2 + (2r^2 - r^4) \left( \frac{7}{64} + \frac{13}{96} \cos 2\theta \right) \right] + O(\delta_0^2). \quad (4.65b)$$

The pressure perturbation  $p_1$ , in (4.63), is

$$p_1 = -\dot{W}_0(t)\phi_1 - (W_0^2/h^2)\kappa s. \quad (4.67)$$

We can now, in principle, calculate the  $O(t)$  perturbations to the boundary layer solutions given in § 4.3.1. There will be a straightforward perturbation to the primary Rayleigh layer (4.57) because of the altered axial core velocity. However, the presence of the  $O(t)$  secondary motions in the core means that there will be secondary motions in the boundary layer from the beginning, with  $v = O(t)$ , which even for a very small value of  $\varepsilon$  might make themselves felt

before those of  $O(t^3)$  driven by centrifugal forces associated with the primary Rayleigh layer. These will also cause a correction to  $w$  at  $O(t^3)$ , not  $O(t^5)$  as in § 4.3.1. Here we restrict our attention to a brief analysis of the  $O(t)$  swirl velocity,  $v$ , and the corrections of  $w$  to  $O(t^3)$ .

The boundary layer equations are (4.53)–(4.56) with  $p'$  not identically zero, but equal to  $\varepsilon\delta'p_1$ , given by (4.67). The outer boundary conditions are now

$$v \sim \varepsilon\delta'W_0\phi_{1\theta}|_{r=1}, \quad w' = (\varepsilon\delta'W_0/h)\phi_{1s} \quad \text{as } \eta \rightarrow \infty.$$

Write

$$v = \varepsilon\delta'\Phi(\theta)\tilde{v}(t, \eta), \quad (4.68a)$$

where

$$\Phi(\theta) = \phi_{1\theta}|_{r=1}, \quad (4.69)$$

and the equation (4.55) becomes a Rayleigh layer equation for  $\tilde{v}$ :

$$\tilde{v}_{\eta\eta} + 2\eta\tilde{v}_{\eta} - 4t(\tilde{v}_t - \dot{W}_0) = O(t^3),$$

with solution

$$\tilde{v} - W_0(t) = -\frac{2}{\sqrt{\pi}} \int_{\eta}^{\infty} W_0\left(t - \frac{t\eta^2}{\mu^2}\right) e^{-\mu^2} d\mu + O(t^3), \quad (4.68b)$$

which is the same as (4.57a) and can be evaluated as in (4.57b). To  $O(t^2)$ ,

$$\tilde{v} - W_0(t) = tw'_0(\eta) + t^2w'_1(\eta).$$

The corresponding correction  $\tilde{u}'$  to the normal velocity  $u'$  is, from (4.53), given by

$$\frac{1}{(4t)^{1/2}}\tilde{u}'_{\eta} = \varepsilon\delta'\left[\Phi'(\theta) - \frac{\delta_0 \sin \theta}{h}\Phi(\theta)\right]\tilde{v}(t, \eta). \quad (4.70)$$

The first corrections to  $w'$  are of two kinds. One is needed to account for the correction to the axial velocity in the core, and can be effected by multiplying (4.57a or b) by  $1 + \varepsilon\delta'\phi_{1s}$  ( $= 1 + \varepsilon\delta'\kappa s$  from (4.65a)); here  $w'$  is taken to be the difference between  $w$  and the *corrected* core velocity. These constitute corrections at  $O(t)$  and  $O(t^2)$ . The other kind of correction involves terms at  $O(t^3)$  and  $O(t^4)$ , driven by  $\tilde{v}$  via  $\tilde{u}$ . If this correction is written as

$(\varepsilon\delta'/h)\tilde{w}'(t, \theta, \eta)$ , (4.56) gives

$$\begin{aligned} \tilde{w}'_{\eta\eta} + 2\eta\tilde{w}'_{\eta} - 4t\tilde{w}'_t = & - \left[ \Phi'(\theta) - \frac{\delta \sin \theta}{h} \Phi(\theta) \right] \\ & \times 4t^2(w'_{0\eta} + tw'_{1\eta}) \int_0^\eta \tilde{v} \, d\eta + O(t^5), \end{aligned} \quad (4.71)$$

where the product of the  $O(t^2)$  term in  $\int \tilde{v} \, d\eta$  with the  $O(t)$  term in the preceding bracket is not to be calculated, being incorporated into the  $O(t^5)$  term.

Equation (4.71) has also been integrated, subject to the usual boundary conditions, by Farthing (1977), and he has found that the correction to the axial component of dimensionless wall shear stress is

$$\left(\frac{Re}{4t}\right)^{1/2} \frac{\varepsilon\delta'}{h} \left[ \Phi'(\theta) - \frac{\delta \sin \theta}{h} \Phi(\theta) \right] \frac{t^3}{t_1^3} \left( 1.45 - 2.43 \frac{t}{t_1} \right). \quad (4.72a)$$

As yet this can be evaluated only to  $O(\delta_0)$ , from (4.69) and (4.65*b*), whence  $1/h$  times the square bracket is equal to

$$\frac{1}{4} [\cos \theta - \frac{19}{6} \delta_0 (1 - \frac{26}{19} \sin^2 \theta) + O(\delta_0^2)]. \quad (4.72b)$$

These results show that when  $\delta$  is increasing (and small) the axial wall shear initially increases on  $\theta = 0$  and decreases on  $\theta = \pi$ . This is due to the thinning of the boundary layer at  $\theta = 0$  and the thickening at  $\theta = \pi$  consequent upon the normal inflow/outflow there: as  $\eta \rightarrow \infty$  an integration of (4.70) yields

$$\frac{1}{(4t)^{1/2}} \tilde{u}' \sim \varepsilon\delta' \left[ \Phi'(\theta) - \frac{\delta_0 \sin \theta}{h} \Phi(\theta) \right] \frac{t}{t_1} \left( 18.5 - 18.8 \frac{t}{t_1} \right),$$

which is initially positive when  $\delta_0$  is small,  $\delta'$  is positive and  $\theta = 0$ . Later, when  $t/t_1 \approx 0.6$ , the sign of the correction to the axial wall shear stress is predicted to change, from (4.72*a*), but the small- $t$  expansions are almost certainly invalid by then (see § 4.3.1). Note that at  $\theta = \pm \frac{1}{2}\pi$ , where  $\cos \theta = 0$ , the  $\sin^2 \theta$  term in (4.72*b*) indicates an initial slight increase in wall shear when  $\delta' > 0$ . These effects are independent both of the uniform decrease in shear associated with the deceleration of the axial velocity in the core as  $\delta$  increases

(from the  $\frac{1}{2}\kappa s^2$  term in (4.65a), since  $\kappa < 0$ ) and of the deceleration/acceleration at the outer/inner wall consequent upon the change in  $h$  as  $\delta_0$  increases.

Farthing (1977) has taken the above expansions somewhat further, and has also examined the effect of torsion of the tube axis, which is not negligible in the aorta. He made calculations for a tube with a right-handed twist, from the point of view of an observer looking along the tube in the downstream direction with the instantaneous plane of curvature horizontal and with the centre of curvature to the right. He found, not unexpectedly, that a right-handed spiral motion was superimposed on the whole flow, resulting in a deceleration of the axial flow in the top half of the tube and an acceleration in the bottom half. The axial wall shear was decreased in the top half and increased in the bottom half, while the reverse was true of the azimuthal wall shear.

#### 4.4 Entry flow with a flat entry profile

The analysis of the previous section has taken the theory of steady and unsteady fully developed flow in a curved tube about as far as possible without a major numerical effort, involving the full Navier-Stokes equations, not boundary layer approximations to them. We still lack a complete description of the flow for values of  $\delta$  that are not vanishingly small, except during the early part of systole, just after the motion begins. Nevertheless, the main qualitative features of the flow, including the initiation of secondary motions and the consequent modification of the axial velocity profile, are fairly clear. This section is devoted to flow near the entrance of a curved tube, and the aim is to extend the unsteady theory of § 3.2 to take account of (possibly non-uniform) vessel curvature. Far downstream from the entrance, the flow is expected to tend to one of the fully developed flows already described. This section is concerned with steady or unsteady flow that enters a curved tube from a reservoir of uniform total pressure, with an effectively flat velocity profile; this may be applicable to the entrance to the aorta, and there are model experiments in uniformly curved tubes with which the theory can be compared. The next section examines steady flow in a tube that is initially straight (and contains Poiseuille

flow) but starts curving at some given point. This example is included not because there is an immediate application to a particular artery, but because (a) it sheds light on the interaction between Poiseuille flow and non-uniformities in the tube, a problem that is examined further in the following chapter on branching tubes, and (b) it can be extended to analyse the flow in a tube that becomes straight after experiencing a bend, as in the descending aorta.

Here we suppose the flow to enter the tube from a reservoir of uniform total pressure, so that the inviscid core flow is expected to be the same irrotational flow as that already derived for a fully developed flow starting from rest. Thus in the core, using the same non-dimensionalisation as in § 4.3, and considering a tube with non-uniform curvature  $\delta(\varepsilon s)$ , we have from (4.62), to  $O(\varepsilon)$ ,

$$(u_c, v_c, w_c) = \left[ 0, 0, \frac{W_0(t)}{h_0} \left( 1 - \frac{\varepsilon s \delta'_0 r \cos \theta}{h_0} \right) \right] + \varepsilon \delta'_0 W_0(t) \nabla \phi_1, \quad (4.73)$$

where  $h_0 = 1 + \delta_0 r \cos \theta$ ,  $\delta_0 = \delta(0)$ ,  $\delta'_0 = \delta'(0)$  and  $\phi_1$  is given to  $O(\delta_0)$  by (4.65b). The entrance to the tube is at  $s = 0$  and a suffix 'c' refers to the inviscid core. For the case of uniform curvature  $\delta_0$ , this reduces to  $[0, 0, W_0(t)/h_0]$ . The corresponding pressure is, from (4.51) and (4.66),

$$p_c = -s \dot{W}_0(t) - \frac{W_0^2(t)}{2h_0^2} - \varepsilon \delta'_0 \left[ \dot{W}_0(t) \phi_1 + \frac{W_0^2(t)s}{h_0^2} \left( \kappa - \frac{r \cos \theta}{h_0} \right) \right]. \quad (4.74)$$

We shall confine attention to functions  $W_0(t)$  that are positive for extended periods of time, so that an approximately quasi-steady flow can be realised.

The mechanism by which secondary motions are generated, and the axial flow modified, as  $s$  increases is physically very similar to the mechanism described above for  $s$ -independent flow as  $t$  increases. For the moment consider constant and uniform  $\delta$ . For very small  $s$ , the primary action of viscosity is to generate a Blasius boundary

layer in which the axial velocity, in (4.73), is reduced to zero. At a given point on the tube wall, this will have thickness  $\tilde{\Delta}$  proportional to  $[\nu s_1(s, \theta)/W_\infty(s, \theta)]^{1/2}$  where  $s_1$  is the distance to the point in question, greater along the outside wall of the tube than the inside, and  $W_\infty$  is the axial velocity just outside the boundary layer, equal to  $w_c|_{r=1}$  and greater on the inner wall. Thus the wall shear, proportional to  $W_\infty/\tilde{\Delta}$ , will be greater on the inner wall. However, the transverse pressure gradient ( $p_{cr}$ ,  $p_{c\theta}/r$ ), required to balance the centrifugal force in the core, also acts on the more slowly moving fluid in the Blasius boundary layer and generates a secondary velocity  $v$  there, from the outside of the bend to the inside. This has the effect of relatively thinning the boundary layer at the outside and thickening it at the inside, so that after a certain distance the shear distribution may be expected to reverse and to tend towards that in steady flow. This has been confirmed by the detailed boundary layer analysis of Singh (1974). We here reproduce the essential elements of Singh's analysis, modified so as not to require vanishingly small  $\delta$ , and extended to take account of unsteady flow and non-uniform curvature. Both extensions are important in the aorta, because the flow is highly unsteady and because the ascending aorta is not very greatly curved initially, the main curvature of the arch developing after 2 or 3 cm.

The full governing equations are again (4.1)–(4.4), with  $Re$  again taken to be large. We transform them to the boundary layer form appropriate for quasi-steady flow (§ 3.2) by changing the variables as follows:

$$\begin{aligned}\eta &= Re^{1/2}[(1-r)/h_0][W_0(t)/2s]^{1/2}, \\ u &= (Re^{-1/2}/h_0)[W_0(t)/2s]^{1/2}u_1, \quad v = W_0(t)v_1, \quad (4.75) \\ w &= [W_0(t)/h_0]w_1, \quad h_0 = 1 + \delta_0 \cos \theta.\end{aligned}$$

The inclusion in these scales of the  $\theta$ -dependent factor  $h_0$  incorporates the facts that both  $W_\infty$  and  $1/\tilde{\Delta}$  are larger at the outside of the bend than the inside, and mean that the leading order Blasius flow is a function only of  $\eta$ . This greatly simplifies the subsequent analysis (like the inclusion of  $W_0(t)$  to describe quasi-steady flow). Failure to make this choice of scaling was probably the reason why Singh (1974) confined his analysis to small values of  $\delta_0$ .

The governing equations now are

$$\begin{aligned}
 u_{1\eta} + \eta w_{1\eta} - 2sw_{1s} &= 2sh_0^2 \left[ v_{1\theta} + \frac{\delta_0 \sin \theta}{h_0} (\eta v_{1\eta} - v_1) \right] \\
 &\quad + \frac{\varepsilon s \delta'_0 \cos \theta}{h_0} (\eta w_{1\eta} - 2sw_{1s}) \\
 &\quad - 2\varepsilon \delta'_0 s^2 \sin \theta v_1, \quad (4.76)
 \end{aligned}$$

$$\begin{aligned}
 w_{1\eta\eta} + u_1 w_{1\eta} + w_1 (\eta w_{1\eta} - 2sw_{1s}) &- \frac{2sh_0^2}{W_0^2(t)} p_{cs} \\
 &= 2sh_0^2 \left[ \frac{\dot{W}_0}{W_0^2} (w_1 + \frac{1}{2} \eta w_{1\eta}) + \frac{\dot{w}_1}{W_0} + v_1 \left( w_{1\theta} + \frac{\delta_0 \sin \theta}{h_0} \eta w_{1\eta} \right) \right] \\
 &\quad + \frac{\varepsilon s \delta'_0 \cos \theta}{h_0} w_1 (\eta w_{1\eta} - 2sw_{1s}) - 2\varepsilon s^2 \delta'_0 \sin \theta v_1 w_1, \quad (4.77)
 \end{aligned}$$

$$\begin{aligned}
 v_{1\eta\eta} + u_1 v_{1\eta} + w_1 (\eta v_{1\eta} - 2sv_{1s}) &- \frac{2sh_0^2}{W_0^2(t)} p_{c\theta} \\
 &= 2sh_0^2 \left[ \frac{\dot{W}_0}{W_0^2} (v_1 + \frac{1}{2} \eta v_{1\eta}) + \frac{\dot{v}_1}{W_0} + v_1 \left( v_{1\theta} + \frac{\delta_0 \sin \theta}{h_0} \eta v_{1\eta} \right) \right. \\
 &\quad \left. + \frac{\delta_0 \sin \theta}{h_0^3} w_1^2 \right] \\
 &\quad + \frac{\varepsilon s \delta'_0 \cos \theta}{h_0} w_1 (\eta v_{1\eta} - 2sv_{1s}) + 2\varepsilon s^2 \delta'_0 \sin \theta \frac{w_1^2}{h_0^2}. \quad (4.78)
 \end{aligned}$$

In the last two equations, the pressure terms can be derived from (4.74), and include both  $O(1)$  and  $O(\varepsilon)$  terms. The other  $O(\varepsilon)$  terms arise because, in (4.1)–(4.4),  $\delta$  and  $h$  are not equal to  $\delta_0$  and  $h_0$  respectively. The boundary conditions are that  $w$  and  $v$  should tend to  $w_c$ ,  $v_c$ , from (4.73), as  $\eta \rightarrow \infty$ , and  $u$ ,  $v$ ,  $w$  are all zero on  $\eta = 0$ .

The scaling has been performed in such a way that, as  $s \rightarrow 0$  and for  $\varepsilon = 0$ , the solution is obviously the Blasius solution,

$$w_1 = w_{10}(\eta) = f'_0(\eta), \quad u_1 = u_{10}(\eta) = f_0 - \eta f'_0, \quad v_1 = 0. \quad (4.79)$$

For non-zero but small  $s$  and  $\varepsilon$ , let us write

$$\begin{aligned}w_1 &= w_{10}(\eta) + \sum_{n=1}^{\infty} s^n (w_{1n} + \varepsilon \bar{w}_{1n} + \cdots), \\u_1 &= u_{10}(\eta) + \sum_{n=1}^{\infty} s^n (u_{1n} + \varepsilon \bar{u}_{1n} + \cdots), \\v_1 &= \varepsilon \bar{v}_{10}(\eta, \theta) + \sum_{n=1}^{\infty} s^n (v_{1n} + \varepsilon \bar{v}_{1n} + \cdots),\end{aligned}\tag{4.80}$$

where the leading terms for  $w_1$  and  $u_1$  are the Blasius solution. However, there is an  $O(\varepsilon)$  swirl velocity to account for (a) the outer boundary condition

$$v_1 \rightarrow \varepsilon \delta'_0 \Phi(\theta) \quad \text{as } \eta \rightarrow \infty,$$

where  $\Phi(\theta)$  is defined by (4.68), and (b) the corresponding term in the azimuthal pressure gradient  $p_{c\theta}$ . Writing

$$\bar{v}_{10} = \delta'_0 \Phi(\theta) g(\eta) \tag{4.81}$$

and substituting into (4.78), we see that  $g(\eta)$  satisfies

$$g'' + f_0 g' = 0, \quad g(0) = 0, \quad g(\infty) = 1,$$

which has the unique solution  $g(\eta) = f'_0(\eta)$ .

#### 4.4.1 Uniform curvature

We consider first the  $\varepsilon = 0$  solutions for  $s > 0$ . The first corrections to the axial and radial velocities,  $w_{11}$  and  $u_{11}$ , turn out to be zero in steady flow. In unsteady flow they are the same as in a straight tube or on a flat plate, and were calculated in § 3.2.2. In the notation of this section the solution is

$$\begin{aligned}w_{11} &= \frac{h_0^2(\theta) \dot{W}_0(t)}{W_0^2(t)} f'_{11}(\eta), \\u_{11} &= \frac{h_0^2(\theta) \dot{W}_0(t)}{W_0^2(t)} (3f_{11} - \eta f'_{11}),\end{aligned}\tag{4.82}$$

with  $f_{11}(\eta)$  given by (3.13).

Even in steady flow, a swirl velocity  $sv_{11}$  develops at  $O(s)$ . This is given by

$$v_{11} = \frac{\delta_0 \sin \theta}{h_0} g_{11}(\eta), \tag{4.83}$$



where

$$g''_{11} + f_0 g'_{11} - 2f'_0 g_{11} = 2(f_0'^2 - 1), \quad g_{11}(0) = g_{11}(\infty) = 0.$$

This equation was solved numerically by Singh (1974), but he did not report the value of  $g'_{11}(0)$  ( $>0$ ), required for a knowledge of secondary shear stress. Farthing (1977) has recomputed the function, and finds  $g'_{11}(0) = 1.54$ . Note that (4.83) differs from Singh's  $O(s)$  swirl velocity only through the factor  $1/h_0$ , although no assumption of small  $\delta_0$  has been made.

The first effect of curvature on the axial and radial velocities (in the case  $\varepsilon = 0$  still) comes in at  $O(s^2)$  in the terms  $w_{12}$ ,  $u_{12}$ . These terms satisfy

$$\begin{aligned} u_{12\eta} + \eta w_{12\eta} - 4w_{12} &= 2h_0\delta_0 \cos \theta g_{11} + 2\delta_0^2 \sin^2 \theta \eta g'_{11}, \\ w_{12\eta\eta} + f_0 w_{12\eta} + (\eta f_0'' - 4f_0') w_{12} + f_0'' u_{12} \\ &= (h_0^4 \dot{W}_0^2 / W_0^4)(-3f_{11} f_{11}'' + 2f_{11}'^2 - 2f_{11}' + \eta f_{11}'') \\ &\quad + (2h_0^4 \ddot{W}_0 / W_0^3) f_{11}' + 2\delta_0^2 \sin^2 \theta \eta f_0'' g_{11}, \end{aligned}$$

with the usual boundary conditions. Still there is no important interaction between the unsteadiness and the curvature (this comes in first in the terms  $s^2 v_{12}$  and  $s^3 w_{13}$  etc.), and the solution for  $w_{12}$ ,  $u_{12}$  can be expressed as the sum of three terms, two of which are essentially the same as the  $O(x^2)$  terms in the solution for unsteady flow over a flat plate (§ 3.2.2), and one of which accounts for curvature. We can write:

$$\begin{aligned} w_{12} &= (h_0^4 \dot{W}_0^2 / W_0^4) f'_{21}(\eta) + (h_0^4 \ddot{W}_0 / W_0^3) f'_{22}(\eta) \\ &\quad + \delta_0(h_0 \cos \theta - \delta_0 \sin^2 \theta) f'_{12}(\eta), \\ u_{12} &= (h_0^4 \dot{W}_0^2 / W_0^4)(5f_{21} - \eta f'_{21}) + (h_0^4 \ddot{W}_0 / W_0^3)(5f_{22} - \eta f'_{22}) \quad (4.84) \\ &\quad + \delta_0(h_0 \cos \theta - \delta_0 \sin^2 \theta) \left( 5f_{12} - \eta f'_{12} + 2 \int_0^\eta g_{11} d\eta \right) \\ &\quad + 2\delta_0^2 \sin^2 \theta \eta g_{11}. \end{aligned}$$

The functions  $f_{21}(\eta)$  and  $f_{22}(\eta)$  are the same as those arising in § 3.2.2 in (3.13), and their contributions to the wall shear,  $f_{21}''(0)$  and  $f_{22}''(0)$ , are given in table 3.1. The function  $f_{12}(\eta)$  satisfies the

equation

$$f_{12}''' + f_0 f_{12}'' - 4f_0' f_{12}' + 5f_0'' f_{12} = -2f_0'' \int_0^\eta g_{11} \, d\eta,$$

together with boundary conditions  $f_{12}(0) = f_{12}'(0) = f_{12}'(\infty) = 0$ . This function was computed by Singh (1974), and he obtained  $f_{12}''(0) = 0.256$ ,  $f_{12}(\infty) = 0.522$ . The contributions to the axial and wall shear stress from all the functions  $f_{mk}$ ,  $\bar{f}_{mk}$ ,  $g_{mk}$ ,  $\bar{g}_{mk}$  arising in this section (e.g.  $f_{mk}''(0)$ ,  $g_{mk}'(0)$ ) are listed in table 4.1.

Table 4.1. Contributions to axial ( $f$ ) and azimuthal ( $g$ ) wall shear stress from all functions arising in § 4.4, together with the terms in the expansion (4.80) to which they refer

Term	$w_{10}$	$w_{11}$	$w_{12}$	$w_{12}$	$w_{12}$	$w_{13}$	$w_{13}$
Function $F(\eta)$	$f_0'$	$f_{11}'$	$f_{21}'$	$f_{22}'$	$f_{12}'$	$f_{31}'$	$f_{32}'$
$F'(0)$	0.470	1.200	0.383	-0.664	0.256	-0.839	1.008
Term	$\bar{w}_{11}$	$\bar{w}_{11}$	$v_{11}$	$v_{12}$	$\bar{v}_{10}$	$\bar{v}_{11}$	
Function $F(\eta)$	$\bar{f}_{11}'$	$\bar{f}_{12}'$	$g_{11}$	$g_{12}$	$g$	$\bar{g}_{11}$	
$F'(0)$	0.117	2.886	1.536	-1.196	0.470	1.200	

The first real interaction between curvature and unsteadiness comes in the next terms of each of the series (4.80). The solutions are written below, *excluding* those terms in  $u_{12}$  and  $w_{12}$  that come purely from the  $O(s^3)$  terms in the expansions representing the effect of time-dependence on the flat plate boundary layer (and which are written as 't.d.t.' below). We have

$$\begin{aligned} v_{12} &= \delta_0 h_0 \sin \theta (\dot{W}_0 / W_0^2) g_{12}(\eta), \\ w_{13} &= \delta_0 h_0^2 (h_0 \cos \theta - \delta_0 \sin^2 \theta) (\dot{W}_0 / W_0^2) f_{31}' \\ &\quad + \delta_0^2 h_0^2 \sin^2 \theta (\dot{W}_0 / W_0^2) f_{32}' + \text{t.d.t.}, \end{aligned} \quad (4.85)$$

$$\begin{aligned} u_{13} &= \delta_0 h_0^2 (h_0 \cos \theta - \delta_0 \sin^2 \theta) \frac{\dot{W}_0}{W_0^2} \left( 7f_{31} - \eta f_{31}' + 2 \int_0^\eta g_{12} \, d\eta \right) \\ &\quad + \delta_0^2 h_0^2 \sin^2 \theta \frac{\dot{W}_0}{W_0^2} \left( 7f_{32} - \eta f_{32}' + 2\eta g_{12} - 4 \int_0^\eta g_{12} \, d\eta \right) + \text{t.d.t.}, \end{aligned}$$

where

$$g''_{12} + f_0 g'_{12} - 4f'_0 g_{12} = 2g_{11} f'_{11} - 3f_{11} g'_{11} + 4f'_0 f'_{11} + \eta g'_{11} + 2g_{11},$$

$$f'''_{3k} + f_0 f''_{3k} - 6f'_0 f'_{3k} + 7f''_0 f_{3k} = \mathcal{F}_{3k} \quad (k = 1, 2),$$

$$\mathcal{F}_{31} = 2f'_{12} + \eta f''_{12} - 3f''_{12} f_{11} - 5f'_{11} f_{12} + 6f'_{11} f'_{12}$$

$$- 2f''_{11} \int_0^\eta g_{11} \, d\eta - 2f'_0 \int_0^\eta g_{12} \, d\eta,$$

$$\mathcal{F}_{32} = -4f'_{11} g_{11} + 4f'_0 \int_0^\eta g_{12} \, d\eta,$$

and  $g_{12}, f_{3k}$  all satisfy the usual homogeneous boundary conditions. Numerical solution of these equations yields

$$\begin{aligned} g'_{12}(0) &= -1.196, & f'_{31}(0) &= -0.839, & f'_{32}(0) &= 1.008 \\ f_{31}(\infty) &= -1.665, & f_{32}(\infty) &= 1.589. \end{aligned}$$

In quasi-steady flow ( $s\dot{W}_0/W_0^2 \ll 1$ ) the axial wall shear is proportional to

$$\begin{aligned} -w_r|_{r=1} &= (ReW_0^3/2s)^{1/2} (1/h_0^2) \\ &\quad \times [f''_0(0) + s^2 \delta_0 (h_0 \cos \theta - \delta_0 \sin^2 \theta) f''_{12}(0) + O(s^4)] \\ &= (ReW_0^3/2s)^{1/2} (1/h_0^2) \\ &\quad \times [0.470 + 0.256s^2 \delta_0 (\cos \theta + \delta_0 \cos 2\theta) + O(s^4)]. \end{aligned} \quad (4.86)$$

Because of the factor  $h_0^{-2} = (1 + \delta_0 \cos \theta)^{-2}$ , this is initially greater on the inside wall ( $\theta = \pi$ ) than on the outside wall ( $\theta = 0$ ). However the  $O(s^2)$  term is greater on the outside wall, and (assuming that the  $O(s^4)$  term can be neglected) cross-over is predicted at a value of  $s$  given by

$$s = 1.92(1 - \delta_0^2)^{-1/2}. \quad (4.87)$$

Singh (1974) also found cross-over at  $s \approx 1.9$  in the small- $\delta_0$  limit; the result (4.87), however, makes no assumptions about the smallness of  $\delta_0$  except that  $\delta_0 < 1$ . The above expansion is valid only for small values of  $s$ ; in particular, if  $\delta_0$  is quite small we can expect validity for  $s \ll \delta_0^{-1/2}$ . When  $\delta_0$  is given by its maximum value in the arch of the aorta, about 0.2, the expansion is likely to be qualitatively useful only for  $s \lesssim 2$ , i.e. for about one diameter from the

entrance; the cross-over value (4.87) of  $s$  is in that case predicted to be about 1.95, so the prediction is unlikely to be quantitatively accurate, although it would be for smaller  $\delta_0$ . In the very first part of the aorta,  $\delta_0$  is markedly smaller than 0.2, so the prediction may be accurate, subject to modifications introduced by non-uniformity of curvature.

When the flow is not quasi-steady, additional terms appear in the square brackets in (4.86). Some are the same unsteady flow corrections as were computed in § 3.2.2, multiplied by functions of  $\theta$ ; these terms, times the  $h_0^{-2}$  outside the square bracket, are:

$$s(\dot{W}_0/W_0^2)f''_{11}(0) + s^2 h_0^2 [(\dot{W}_0^2/W_0^4)f''_{21}(0) + (\ddot{W}_0/W_0^3)f''_{22}(0)] + O(s^3).$$

Thus the effect of curvature is felt at  $O(1)$  and at  $O(s^2)$  even without a genuine interaction between curvature and unsteadiness, because of the factors  $h_0^{-2}$  and  $h_0^2$  respectively. The first term that represents the interaction is

$$\begin{aligned} h_0^{-2} \cdot s^3 \delta_0 h_0^2 (\dot{W}_0/W_0^2) [(h_0 \cos \theta - \delta_0 \sin^2 \theta) f''_{31}(0) + \delta_0 \sin^2 \theta f''_{32}(0)] \\ = s^3 \delta_0 (\dot{W}_0/W_0^2) [-0.839 h_0 \cos \theta + 1.847 \delta_0 \sin^2 \theta]. \end{aligned} \quad (4.88)$$

The square bracket here is positive at the inside wall ( $\theta = \pi$ ) and negative at the outside wall ( $\theta = 0$ ); the value of  $\theta$  at which it is zero depends on  $\delta_0$ , but is always less than  $\frac{1}{2}\pi$  (when  $\delta_0 = 0.2$ , for example, it is about  $75^\circ$ ). Thus, when the flow is accelerating ( $\dot{W}_0 > 0$ ), this term is of opposite sign to the  $O(s^2)$  term in (4.86), and therefore tends to inhibit the cross-over of maximum shear predicted above. When the flow is decelerating, on the other hand, this interaction tends to promote cross-over at a smaller value of  $s$ .

The leading terms in the expansion for azimuthal wall shear are proportional to

$$-v_r|_{r=1} = \left(\frac{Re W_0^3}{2s}\right)^{1/2} s \frac{\delta_0 \sin \theta}{h_0^2} \left[ g'_{11}(0) + s \frac{h_0^2 \dot{W}_0}{W_0^2} g'_{12}(0) \right]. \quad (4.89)$$

As one would predict from the physical origin of the secondary motions, this is positive as  $s \rightarrow 0$  for all  $\theta \neq 0, \pi$ . However,  $g'_{12}(0)$  is negative, so the effect of an acceleration of the flow ( $\dot{W}_0 > 0$ ) is to cause the secondary component of wall shear to fall below its steady

value as  $s$  increases. Ultimate reversal would be predicted by (4.89) but validity of the equation for values of  $s$  greater than 1–2 is unlikely.

The above expansion appears to break down when  $s = O(\delta_0^{-1/2})$  because the centrifugal force term which drives the azimuthal motion in (4.78) becomes  $O(\delta_0^{1/2})$ . Hence  $v_1$  also becomes  $O(\delta_0^{1/2})$ , with the consequence that the first term on the left-hand side of the continuity equation (4.76) becomes  $O(1)$ , modifying the basic  $w_1$ ,  $u_1$  boundary layer. Singh (personal communication) has stated that some analytical progress is possible in this region ( $S = s\delta_0^{1/2} = O(1)$ ) when  $\delta_0 \ll 1$ , but he has been unable to compute any results from the intractable non-linear equations that arise (except for a series solution in powers of  $S$  that contains the same terms as the above expansion in powers of  $s$ ).

Yao & Berger (1975) investigated the steady entry flow in a uniformly curved pipe (at large values of the Dean number) by a complicated momentum integral method. However the fully developed flow to which their solution was made to tend was assumed to have parallel secondary streamlines in the core (as in the attempted solution by Barua (1963)), and this overspecifies the problem as shown in § 4.1.3 (it is equivalent to assuming  $w'_c(x) \equiv 1$  in (4.24)). Thus their results show separated secondary flow, unlike the fully developed momentum integral solution of Ito (1969), which would have been a better downstream limit.

Yao & Berger's analysis leads to a prediction of entry length  $\hat{s}_e$  approximately proportional to  $aRe^{1/2}\delta^{-1/4}$  (compared with  $aRe$  in a straight tube;  $Re = \hat{W}_0 a/\nu$ ). This scaling can be deduced as follows. The simplest order-of-magnitude argument suggests that the entry length should be the value of  $\hat{s}$  at which the thickness of the Blasius boundary layer at the entrance,  $\propto (\nu\hat{s}/\hat{W}_0)^{1/2}$ , is comparable with that in fully developed, large-Dean-number flow far downstream,  $\propto aD^{-1/3}$ . Now  $\hat{W}_0$  is related to  $D$  through the scaling of § 4.1.3, where

$$w' = (2\delta)^{1/2}(a\hat{W}_0/\nu) = O(D^{2/3}). \quad (4.90)$$

This leads to  $\hat{s}_e/a \propto \delta^{-1/2}$ , which is very much smaller than Yao & Berger's estimate, and indeed is equivalent to  $s = O(\delta^{-1/2})$ , where

Singh's (1974) entry solution first breaks down. However, this simple prediction fails to account for the time required for the transport of secondary vorticity from the boundary layer into the core, which will require a time of  $a/\hat{V}$  to develop, where  $\hat{V}$  is a scale for the secondary velocity in the core. Hence a distance of  $\hat{W}_0 a/\hat{V}$  will be needed. Now  $\hat{V} = (\nu/a)D^{1/3}$  (see § 4.1.3), so this gives

$$\hat{s}_e/a = \hat{W}_0/\hat{V} = Re/D^{1/3} = Re^{1/2}\delta^{-1/4} \quad (4.91)$$

from (4.90). The experiments reported in § 4.4.3 below confirm that this estimate of entry length is much nearer the truth than either  $a\delta^{-1/2}$  or  $aRe$ .

#### 4.4.2 Slowly varying curvature

We now turn to the first corrections that must be included in the above expansions in order to describe the effect of non-uniform curvature. These are the terms  $\varepsilon s(\bar{u}_{11}, \bar{v}_{11}, \bar{w}_{11})$  in (4.80). We neither restrict the flow to being quasi-steady, nor do we limit the analysis to small values of  $\delta_0$ . When account is taken of the solutions for  $u_{10}, w_{10}, u_{11}, w_{11}, \bar{v}_{10}$ , given in (4.79), (4.81) and (4.82), the equations for the present variables, from (4.76) to (4.78), are

$$\begin{aligned} \bar{u}_{11\eta} + \eta \bar{w}_{11\eta} - 2\bar{w}_{11} &= \eta f_0''(\eta)(\delta_0'/h_0)[\cos \theta + 2h_0^2\delta_0 \sin \theta \Phi(\theta)] \\ &\quad + f_0'(\eta)2\delta_0'h_0^2\left[\Phi'(\theta) - \frac{\delta_0 \sin \theta}{h_0}\Phi(\theta)\right], \\ \bar{w}_{11\eta\eta} + f_0\bar{w}_{11\eta} + (\eta f_0'' - 2f_0')\bar{w}_{11} + f_0''\bar{u}_{11} + 2\delta_0'\left(\kappa - \frac{\cos \theta}{h_0}\right) \\ &= \eta f_0'f_0''(\delta_0'/h_0)[\cos \theta + 2h_0^2\delta_0 \sin \theta \Phi(\theta)], \\ \bar{v}_{11\eta\eta} + f_0\bar{v}_{11\eta} - 2f_0'\bar{v}_{11} &= \delta_0'h_0^2[\dot{W}_0(t)/W_0^2(t)]\Phi(\theta) \\ &\quad \times [-3f_0''f_{11} + 2(f_0' - 1) + \eta f_0''], \end{aligned}$$

with the usual boundary conditions at  $\eta = 0$ , and

$$\bar{w}_{11} \rightarrow \delta_0'\left(\kappa - \frac{\cos \theta}{h_0}\right), \quad \bar{v}_{11} \rightarrow 0 \quad \text{as } \eta \rightarrow \infty.$$

We recall that  $\Phi(\theta)$  is given by (4.69) and (4.65), while  $\kappa$  is given by (4.66); these quantities represent the perturbation to the irrotational core flow. These equations have the following solutions:

$$\left. \begin{aligned} \bar{w}_{11} &= \delta'_0 \left[ \frac{\cos \theta}{h_0} + 2h_0^2 \Phi'(\theta) \right] \bar{f}'_{11}(\eta) + \delta'_0 \left( \kappa - \frac{\cos \theta}{h_0} \right) \bar{f}'_{12}(\eta), \\ \bar{u}_{11} &= \delta'_0 \left[ \frac{\cos \theta}{h_0} + 2h_0^2 \Phi'(\theta) \right] (3\bar{f}_{11} - \eta \bar{f}'_{11}) \\ &\quad + (\delta'_0/h_0) [\cos \theta + 2h_0^2 \delta_0 \sin \theta \Phi(\theta)] (\eta f'_0 - f_0) \\ &\quad + 2\delta'_0 h_0^2 \left[ \Phi'(\theta) - \frac{\delta_0 \sin \theta}{h_0} \Phi(\theta) \right] f_0(\eta) \\ &\quad + \delta'_0 \left( \kappa - \frac{\cos \theta}{h_0} \right) (3\bar{f}_{12} - \eta \bar{f}'_{12}), \\ \bar{v}_{11} &= \delta'_0 h_0^2 \Phi(\theta) (\dot{W}_0(t)/W_0^2(t)) \bar{g}_{11}(\eta), \end{aligned} \right\} \quad (4.92)$$

where the functions  $\bar{f}_{11}$  and  $\bar{f}_{12}$  satisfy

$$\begin{aligned} \bar{f}'''_{1k} + f_0 \bar{f}''_{1k} - 2f'_0 \bar{f}'_{1k} + 3f''_0 \bar{f}_{1k} &= -f_0 f''_0 \quad (k=1) \\ &= -2 \quad (k=2) \end{aligned} \quad (4.93)$$

and  $\bar{g}_{11}$  satisfies

$$\bar{g}''_{11} + f_0 \bar{g}'_{11} - 2f'_0 \bar{g}_{11} = -3f''_0 f_{11} + 2(f'_0 - 1) + \eta f''_0. \quad (4.94)$$

The outer boundary conditions are

$$\bar{f}'_{11}(\infty) = 0, \quad \bar{f}'_{12}(\infty) = 1, \quad \bar{g}_{11}(\infty) = 0;$$

the solution for  $\bar{g}_{11}$  is  $\bar{g}_{11} \equiv f'_{11}$ , from (3.13). Numerical solution of the equations for  $\bar{f}_{11}$  and  $\bar{f}_{12}$  yields  $\bar{f}'_{11}(0) = 0.117$ ,  $\bar{f}'_{12}(0) = 2.886$ . Finding later terms in the expansion (4.80) can be reduced to the solution of ordinary differential equations in a similar way, but the labour rapidly becomes prohibitive.

These solutions result in additional contributions to the axial and azimuthal components of wall shear, in (4.86) and (4.89) respectively. Since  $\Phi(\theta)$  is known only to  $O(\delta_0)$  (from (4.69) and (4.65)), we present the results only to that order. The first correction to the square brackets of (4.86), multiplied by  $h_0^{-2}$ , is

$$\varepsilon \delta'_0 [-2.71 \cos \theta + \delta_0 (-1.32 + 8.06 \cos^2 \theta) + O(\delta_0^2)]. \quad (4.95)$$

The first term here has the same sign as that in (4.88), so, if  $\delta_0$  is small, a gradual increase in curvature has a similar effect as an acceleration of the core flow, and tends to inhibit the cross-over of maximum shear. For larger values of  $\delta_0$ , (4.95) suggests that the increase in curvature would tend to increase the wall shear on both the outside and the inside walls of the bend, reducing it on the side-walls ( $\theta = \pm \frac{1}{2}\pi$ ). However, the expansion in powers of  $\delta_0$  would be invalid if the second term became as large as the first ( $\delta_0 \approx 0.34$ ). It no doubt gives qualitatively correct results for  $\delta_0 \leq 0.2$ , the value in the aorta.

The corrections introduced by variable curvature into the azimuthal wall shear consist of the following additions to (4.89):

$$(Re W_0^3/2s)^{1/2} [\varepsilon \delta'_0 \Phi(\theta)/h_0] [0.47 + 1.20 sh_0^2 (\dot{W}_0/W_0^2)],$$

where

$$\Phi(\theta) = \frac{1}{4} \sin \theta - \frac{13}{48} \delta_0 \sin 2\theta + O(\delta_0^2).$$

Thus if  $\delta'_0 > 0$  and  $\delta_0$  is small, we see that an increase in curvature enhances the leading term of (4.89), i.e. increases the azimuthal wall shear at  $\theta = \frac{1}{2}\pi$ , while it reduces the effect of the second term (since  $g'_{12}(0) < 0$ ), and therefore inhibits the tendency for secondary flow reversal during an acceleration of the core.

Having developed the above expansions (and having taken them even further), Farthing (1977) constructed a composite picture of wall shear near the entrance to a rigid tube whose geometry approximated as closely as possible to that of the dog's aorta, as measured from arteriograms taken by Ettinger & Suter (1970). The tube consisted of two segments, of different diameters: the first had diameter 1.5 cm and represented the ascending aorta, while the second had diameter 1.0 cm and represented the descending thoracic aorta. The change in cross-sectional area is a real phenomenon (cf. fig. 1.4), and is related to the fact that a significant proportion of the blood flow leaves through the branches at the arch. It was therefore plausible for Farthing to assume that the cross-sectionally-averaged velocity in the aorta was the same function of time in each segment, although there is no direct evidence in support of this. The waveform  $W_0(t)$  was taken to be a polynomial fit to one measured by Clark & Schultz (1973). It is



more complicated than the crude approximation (4.49), but is not qualitatively different during the period of forward flow,  $0 \leq t \leq t_1$ .

Farthing further assumed that the presence of the branches has no effect on the flow near the inside wall of curvature, and its effect near the outer wall can be represented by starting a new quasi-steady boundary layer at the last flow divider. This is a gross assumption, but enabled Farthing to continue his expansions downstream of the branches. Each of the aortic segments was taken to have variable curvature, as shown in fig. 4.12(a), where the values of  $\delta(s)$  are given at each cross-section; torsion was also included in the model.

Farthing used the small- $s$  expansions of this section to give the approximately quasi-steady flow near the entrance to the aorta, and the small- $t$  expansion of the previous section to give the downstream diffusive flow to which it must match. He found that the most convenient way of effecting the match was to use an extended version of the modified Oseen approximation of Lewis & Carrier (1949) (cf. p. 154). Some of his results are shown in fig. 4.12(a)–(d). In each part of the figure, the aortic wall is viewed from the animal's left side, as if it were untwisted and flattened, retaining the curvature of the inside wall (the outside wall is therefore somewhat stretched). Then at five points on each cross-section chosen, the computed shear stress on the far wall is represented as a vector; where the stress on the near wall is different (on account of the slight torsion) it is represented by a second vector. The four parts of fig. 4.12 represent four times during the cycle,  $0.1T$ ,  $0.2T$ ,  $0.3T$  and  $0.5T$  respectively, where  $T$  is the total period of the cycle (the time  $t_1$  at which the entering core flow first reverses is approximately  $0.6T$  on this scale). At  $0.1T$ , the flow is purely diffusive; the axial component of wall shear is greater towards the inside of the bend, consistent with the potential vortex core flow (4.50); a small azimuthal component of shear can be seen to have developed near the region of maximum tube curvature. At  $0.2T$  the secondary motion has become much stronger, and the axial component of shear near the entrance is greater than that further downstream because of the quasi-steady influence of the leading edge. At  $0.3T$ , just after the peak in the entering core flow, flow reversal has occurred at the inside wall of the arch, and the secondary components of shear near

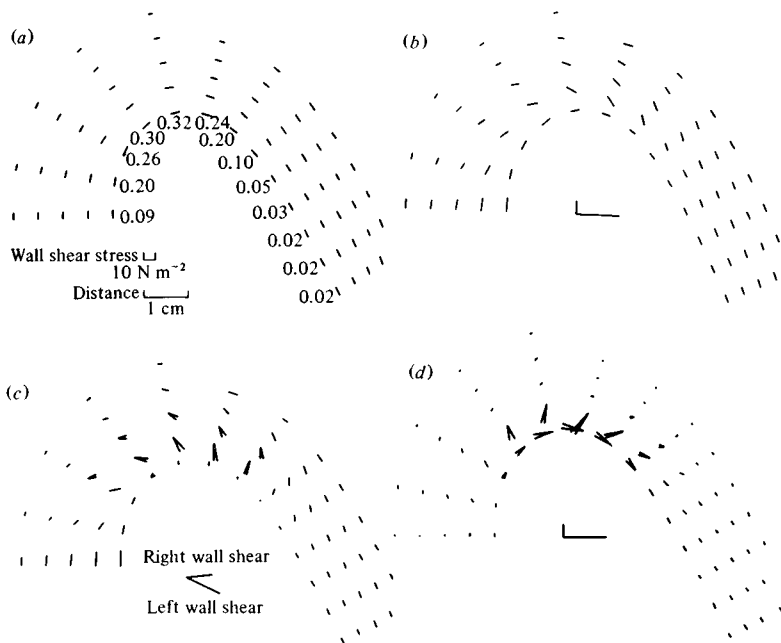


Fig. 4.12. Predictions of wall shear stress in the upper part of a dog's aorta. The aortic wall is viewed from the animal's left side, as if it were untwisted and flattened, retaining the curvature of the inside wall. Numbers by each cross-section in (a) represent the value of the local curvature ratio  $\delta$ . The shear on the far wall at each point is represented by a vector; where the shear at the near wall is different (because of torsion) it is represented by a second vector. The different panels represent different times during the cycle (total period,  $T$ ): (a)  $0.1T$ , (b)  $0.2T$ , (c)  $0.3T$ , (d)  $0.5T$ . (After Farthing, 1977.)

maximum curvature exceed all others. This suggests a breakdown of the small- $t$  expansion, as foreseen above. The effect of torsion is just noticeable. At  $0.5T$  the axial flow in the boundary layer has reversed almost everywhere, but the predicted shear values cannot be expected to be accurate.

These calculations represent the furthest that one can go in making analytical predictions of wall shear in the aorta. Since the curvature ratio  $\delta$  is not taken to be vanishingly small, nor to be uniform ( $\epsilon \neq 0$ ), the present approach is likely to give more realistic quantitative information than any other. The big defects of the theory, however, are that it can be accurate only in the early part of

systole, and only in the ascending aorta where the effects of the branches at the arch are not dominant. Apart from a qualitative understanding of the effects of branches (see chapter 5) future predictions will almost certainly have to be made by fully numerical means.

#### 4.4.3 Experiments

Model experiments have recently been performed on steady entry flow in uniformly curved tubes by two workers. Olson (1971), with air as the working fluid, used a single hot-wire anemometer to measure axial velocity profiles and a double, pulsed wire to measure the secondary velocity field (see § 5.1 for his measurements on branched tubes). Agrawal (1975) used laser-Doppler anemometry to measure the complete velocity field, in water (see also Agrawal, Talbot & Gong, 1978). Agrawal investigated only flat entry profiles (as examined theoretically above), while Olson investigated both flat and parabolic entry profiles (cf. § 4.5).

In the case of the flat entry profile at moderately high Dean numbers, both authors confirmed that, for small  $s$ , the axial velocity profile in the core is slightly skewed towards the inside of the bend, as in the predicted potential vortex flow. This is also consistent with the skewing of the velocity profile in the upper part of the ascending aorta, as shown in fig. 1.22(*b*). They then reported that the core flow was eaten away by the rapid thickening of the boundary layer at the inside of the bend, and that eventually (after about 180° of bend) the axial profile had a peak near the outside of the bend and decreased approximately linearly across the core. Typical profiles are shown in figs. 4.13(*b*) and 4.14(*b*), where qualitative, but not quantitative, agreement can be seen, although the values of  $\delta$  and  $D'$ , where

$$D' = 2(a/R)^{1/2} \hat{W}_0 a / \nu, \quad (4.96)$$

were comparable (in Olson's experiments (fig. 4.14)  $\delta = \frac{1}{16}$  and  $D' = 257$ , in Agrawal's (fig. 4.13)  $\delta = \frac{1}{20}$  and  $D' = 251$ ). Note that here  $D' = \sqrt{2}D^{2/3}$  when  $D$  is defined by (4.9), because  $D'$  is a Dean number based on axial velocity, while  $D$  is based on pressure gradient (see (4.90)). The discrepancy in the results shown lies in the

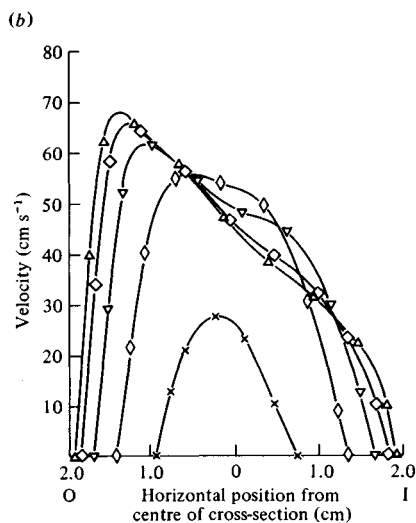
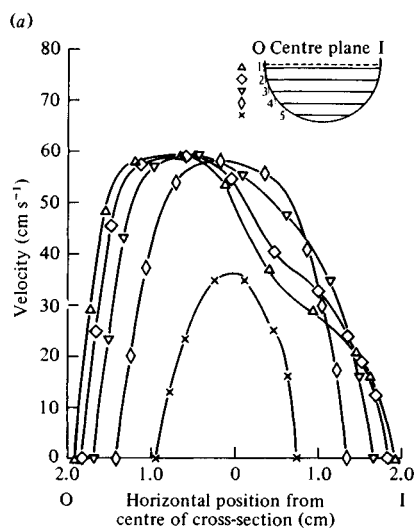
more rapid encroachment of the boundary layer in Agrawal's experiments, since his results at a bend angle of about  $35^\circ$  ( $s = 12.2$ ) are comparable with Olson's at an angle of  $60^\circ$  ( $s = 16.8$ ).

The two authors concur in their conclusion that the flow is virtually fully developed by the last station measured in each case ( $s = 57$  for Agrawal, and  $s = 50$  for Olson). These values are comparable with Yao & Berger's prediction of  $Re^{1/2}\delta^{-1/4}$  from (4.91) (equal to 50 for Agrawal, 46 for Olson) and are much greater than  $\delta^{-1/2}$  and much smaller than  $Re$ .

Figs. 4.13(c), (d) show Agrawal's measurement of the  $x$ -component of secondary velocity ( $x = r \cos \theta$ , measured across the cross-section of the tube in the plane of the bend) at the same downstream stations as the axial profiles in figs. 4.13(a) and (b). They confirm the qualitative picture of a jet-like secondary motion in the boundary layer, from outside to inside of the bend, and a slower drift back across the core; however, the details are more complicated than can be predicted by the theories.

Figs. 4.14(a), (c) and (d) are Olson's measurements for a parabolic entry profile, when the curved tube was fixed to the end of a long straight tube. The flow appears to become fully developed at about the same value of  $s$  as for a flat entry profile (fig. 4.14(a)), when the secondary motions (fig. 4.14(c)) and the contour plot of axial velocity (fig. 4.14(d)) also show good correspondence. The latter, at a value of  $D' = 258$ , corresponding to  $D = 2460$ , shows good qualitative agreement with the theoretical contour plot (at  $D = 5000$ ) shown in fig. 4.2(c). The developing axial profile in fig. 4.14(a) shows that the peak velocity rapidly veers to the outside of the bend, in contrast to the case of a flat entry profile. This is consistent with a model in which the flow in the centre of the tube carries on undisturbed, while that near the walls is forced around, again in a secondary jet-like boundary layer. This then erupts into the core again at the inside of the bend, where a second maximum in the axial velocity profile occurs at first, subsequently dying away. The initial stages of this development are described by the theory to be presented in § 4.5.

We note finally that neither author made accurate measurements of wall shear in his models.



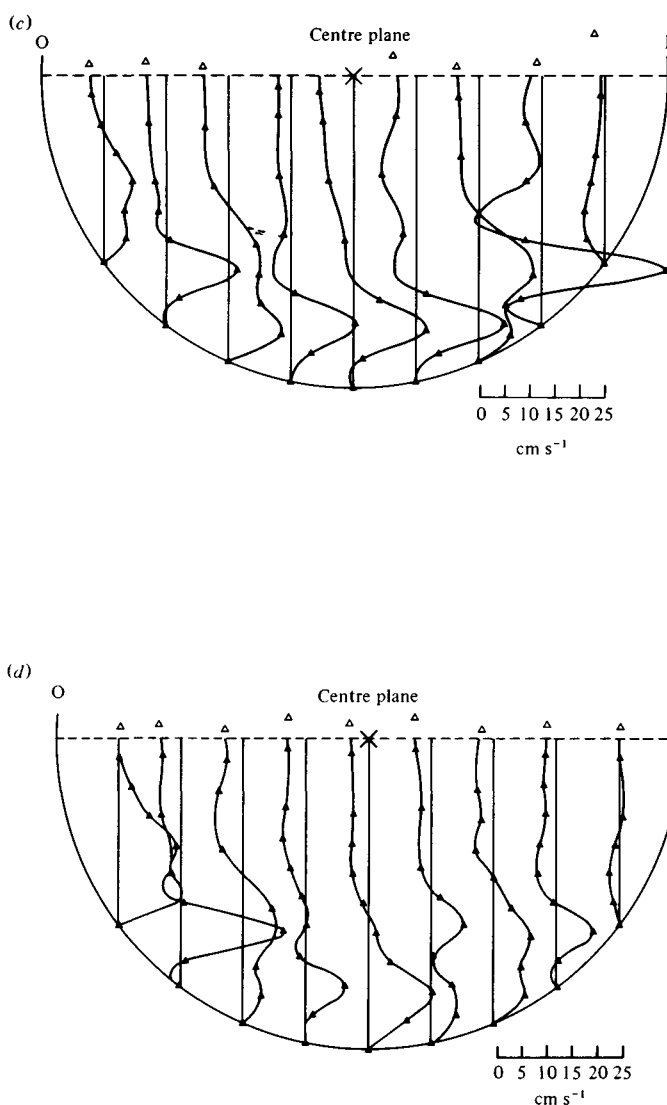
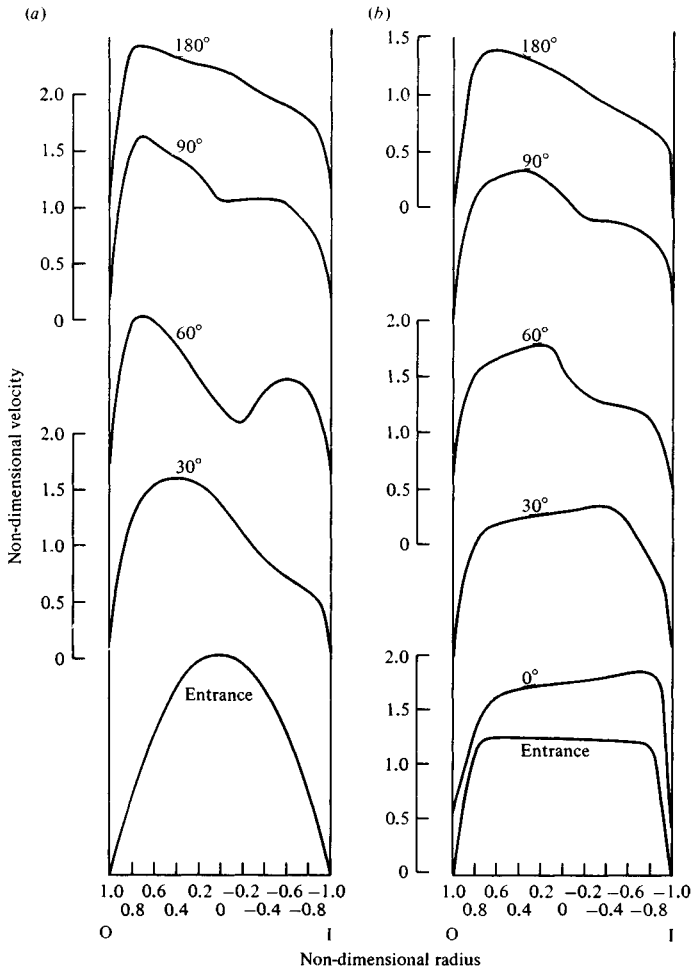


Fig. 4.13. Measurements of entry flow in a curved tube. Axial velocity profiles along horizontal traverses: (a)  $\delta = \frac{1}{20}$ ,  $D' = 251$ ,  $s = 12.2$ ; (b) as (a), but with  $s = 57.2$ . Secondary velocity profiles along vertical traverses: (c)  $\delta = \frac{1}{20}$ ,  $D' = 251$ ,  $s = 12.2$ ; (d) as (c), but with  $s = 57.2$ . (After Agrawal, 1975.) Dr Agrawal has pointed out that some of the wiggles in these profiles are artefacts and were not present in the more recent curves of Agrawal *et al.* (1978).



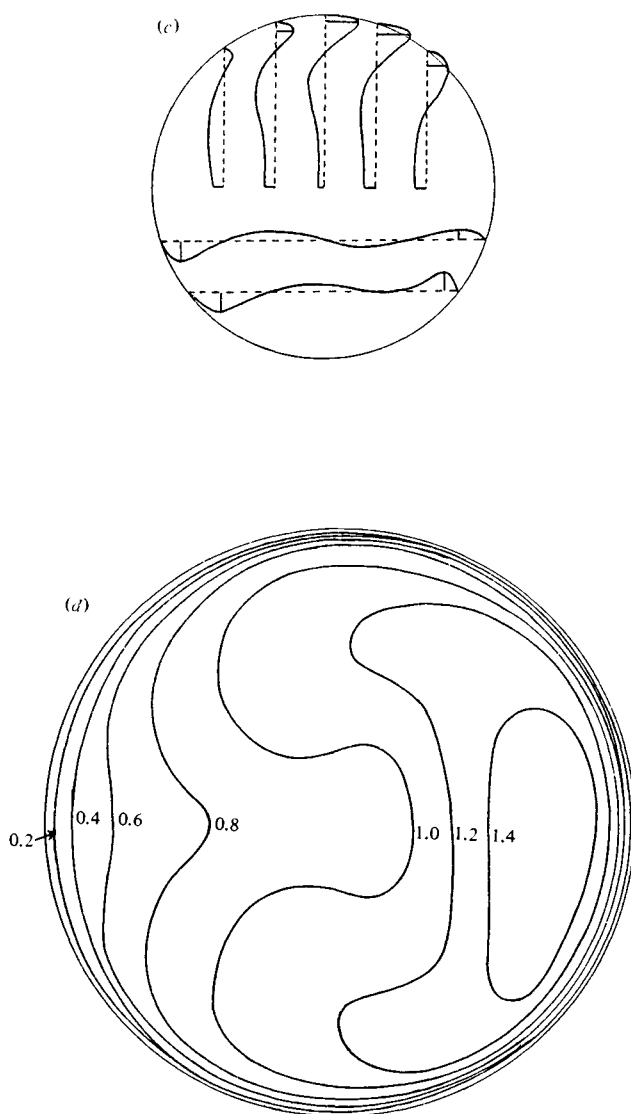


Fig. 4.14. Measured velocity patterns in a curved tube, with  $D' = 258$ ,  $\delta = \frac{1}{16}$ , and  $180^\circ$  of bend (after Olson, 1971). (a) Axial velocity profiles in the plane of the bend; parabolic entry profile. (b) Axial velocity profiles in the plane of the bend; flat entry profile. (c) Transverse velocity profiles after  $180^\circ$  of bend; parabolic entry profile. (d) Contours of axial velocity after  $180^\circ$  of bend; parabolic entry profile.



### 4.5 Steady entry flow with a parabolic entry profile

The theory to be presented here is basically that of Smith (1976*b*), who analysed steady flow in a tube that was straight for  $s < 0$  and had uniform small curvature  $\delta_0$  for  $s > 0$ . He took the Dean number  $D'$ , given by (4.96), to be  $O(1)$  (note that  $D' \propto \delta_0^{1/2} Re$ ), and analysed the flow in the region  $|s| = O(1)$ . His analysis ceases to be valid if either  $D' = O(Re^{5/6})$  or  $s = O(\delta_0^{-1/2}) = O(D'^{-1} Re)$ . Smith took axes  $(r, \theta, s)$  appropriate to the curved tube with fixed curvature  $\delta_0$ , which made a description of the tube wall, and of the undisturbed flow, rather cumbersome for  $s < 0$ . We adhere to axes appropriate to the *local* curvature (equal to 0 in  $s < 0$  and  $\delta_0$  in  $s > 0$  for Smith's case) so that the tube wall is  $r = 1$  for all  $s$ , and extension of the theory to tubes of variable (but small) curvature in  $s > 0$  becomes a simple matter. In particular, it becomes possible to analyse the flow in a tube that suffers a small bend and subsequently becomes straight again. This is expected to give results qualitatively relevant to flow in the descending aorta, where the vessel straightens out after a bend.

If we non-dimensionalise velocities with respect to  $\hat{W}_0$  (the axial velocity-scale) and lengths with respect to  $c$ , the governing equations are again (4.1)–(4.4) with  $Re \gg 1$ , and with the  $\partial/\partial t$  terms absent for steady flow. We describe the (variable) tube curvature by the equation

$$\delta = \delta_0 \Delta(s), \quad \Delta = 0 \quad \text{for } s < 0,$$

where  $\delta_0$  is a suitable scale. We take the Reynolds number to be large, and  $D'$  defined by (4.96) to be  $O(1)$ , so  $\delta_0$  is formally  $O(Re^{-2})$ . Sufficiently far upstream the motion in the straight tube is Poiseuille flow:

$$w = W_0(r) = \frac{1}{4}(1 - r^2), \quad u = v = 0, \quad p = P_0 - s/Re,$$

where  $P_0$  is a given constant. Since the Reynolds number is large and the curvature small, we expect the perturbation to this flow in the core to be inviscid and  $O(\delta_0)$  for  $s = O(1)$ . Far from the tube wall, therefore, we expect the flow field to have the form

$$\begin{aligned} w &= W_0(r) + \delta_0 w_1(s, r, \theta) + o(\delta_0), \\ u &= \delta_0 u_1(s, r, \theta) + o(\delta_0), \end{aligned}$$

$$v = \delta_0 v_1(s, r, \theta) + o(\delta_0),$$

$$p = P_0 - s/Re + \delta_0 p_1(s, r, \theta) + o(\delta_0).$$

Substitution into the governing equations gives the inviscid disturbance equations:

$$u_{1r} + u_1/r + v_{1\theta}/r + w_{1s} = 0,$$

$$W_0 u_{1s} - \Delta \cos \theta W_0^2 = -p_{1r},$$

$$W_0 v_{1s} + \Delta \sin \theta W_0^2 = -p_{1\theta}/r,$$

$$W_{0r} u_1 + W_0 w_{1s} = -p_{1s},$$

with wall boundary condition  $u_1(s, 1, \theta) = 0$ . The unique solution which also matches to the oncoming flow in  $s < 0$  is

$$p_1 = 0, \quad w_1 = -W'_0(r) \cos \theta \int_0^s (s-s') \Delta(s') ds', \quad (4.97)$$

$$u_1 = W_0(r) \cos \theta \int_0^s \Delta(s') ds', \quad v_1 = -W_0(r) \sin \theta \int_0^s \Delta(s') ds'.$$

This means that the Poiseuille flow is not distorted until the bend, and after it the flow carries straight on, not to this order in  $\delta_0$  being diverted by the presence of the bend.

The axial velocity in the core does not satisfy the no-slip condition on the wall, so a viscous boundary layer must be interposed there. Near the wall it is appropriate to rewrite  $W_0$  in the form

$$W_0(r) = \frac{1}{2}(1-r) - \frac{1}{4}(1-r)^2,$$

which is  $O(b)$  if  $b$  is a scale for boundary layer thickness. Then the equation of continuity, (4.1), shows as usual that the scale for  $u$  in the boundary layer is of order  $b$  times the scale for the perturbation in  $w$ . A balance between the leading order inertial and viscous forces in either the swirl or the axial momentum equation then shows that  $b = O(Re^{-1/3})$ . The core flow, from (4.97), also indicates that the perturbation axial velocity is  $O(\delta_0) = O(Re^{-2})$ . We therefore seek a boundary layer expansion in which

$$w = \frac{1}{2}\zeta Re^{-1/3} - \frac{1}{4}\zeta^2 Re^{-2/3} + Re^{-2} w_F(s, \zeta, \theta) + O(Re^{-7/3}),$$

$$u = -Re^{-7/3} u_F(s, \zeta, \theta) + O(Re^{-8/3}),$$

$$v = Re^{-2} v_F(s, \zeta, \theta) + O(Re^{-7/3}),$$

$$p = P_0 - s/Re + Re^{-7/3} p_F(s, \zeta, \theta) + O(Re^{-8/3}),$$

where  $\zeta = Re^{1/3}(1-r)$ . It is crucial to the subsequent solution of the problem (a) that the pressure perturbation  $Re^{-7/3}p_F$  be included, although there is no pressure perturbation to  $O(Re^{-2})$  in the core, and (b) that the swirl velocity  $v$  be  $O(Re^{-2})$  although its core value (4.97) is  $O(Re^{-7/3})$  as  $r \rightarrow 1$ . Without this pressure and swirl velocity no  $u$ - or  $w$ -field of the proposed form could satisfy mass conservation: the Poiseuille flow, impinging on the outside of the bend, must raise the pressure there and force fluid around towards the inside of the bend, as in fully developed flow.

The boundary layer equations governing the motion are

$$\left. \begin{aligned} u_{F\zeta} + v_{F\theta} + w_{Fs} &= 0, \\ 0 &= p_{F\zeta}, \\ \frac{1}{2}\zeta v_{Fs} &= -p_{F\theta} + v_{F\zeta\zeta}, \\ \frac{1}{2}u_F + \frac{1}{2}\zeta w_{Fs} &= -p_{Fs} + w_{F\zeta\zeta}, \end{aligned} \right\} \quad (4.98)$$

and the outer boundary conditions, as  $\zeta \rightarrow \infty$ , are

$$v_F \rightarrow 0, \quad w_F \rightarrow \frac{1}{2}D'' \cos \theta \int_0^s (s-s')\Delta(s') ds', \quad (4.99)$$

where  $D'' = \delta_0 Re^2 (= \frac{1}{4}D'^2$  from (4.96)). Following Smith (1976*b*), we solve these equations by the use of Fourier transforms. We write

$$(w_F, u_F, p_F) = (W, U, P) \cos \theta, \quad v_F = V \sin \theta,$$

where  $U, V, W$  are functions of  $\zeta$  and  $s$  but  $P$  depends only on  $s$ , and define generalised Fourier transforms of the form

$$\tilde{W}(\omega, \zeta) = \int_{-\infty}^{\infty} W(s, \zeta) e^{-i\omega s} ds. \quad (4.100)$$

Eliminating the radial velocity  $U$ , we obtain the following pair of equations for  $\tilde{V}, \tilde{W}, \tilde{P}$ :

$$\left. \begin{aligned} \tilde{W}_{\zeta\zeta\zeta} + \frac{1}{2}\tilde{V} &= \frac{1}{2}i\omega\zeta\tilde{W}_{\zeta}, \\ \tilde{V}_{\zeta\zeta} + \tilde{P}(\omega) &= \frac{1}{2}i\omega\zeta\tilde{V}. \end{aligned} \right\} \quad (4.101)$$

The homogeneous parts of these equations can be reduced to Airy's equation by the substitution

$$t = (0 + \frac{1}{2}i\omega)^{1/3}\zeta,$$

where the notation implies that  $(0 + \frac{1}{2}i\omega)^{1/3}$  has a branch cut extending from  $i0+$  along the positive imaginary  $\omega$ -axis. The solution of

(4.101) satisfying the conditions that  $\tilde{V}$  vanishes at  $\zeta = 0$  and as  $\zeta \rightarrow \infty$  is

$$\left. \begin{aligned} \tilde{V}(\omega, \zeta) &= -(0 + \tfrac{1}{2}i\omega)^{-2/3} \tilde{P}(\omega) L(t), \\ \text{where} \quad L(t) &= Ai(t) \int_0^t \frac{dq}{Ai^2(q)} \int_\infty^q Ai(\xi) d\xi \end{aligned} \right\} \quad (4.102)$$

and  $Ai$  is the Airy function. Then, from (4.101), the solution for  $\tilde{W}$  that is zero at  $\zeta = 0$  and bounded as  $\zeta \rightarrow \infty$  is given by

$$\tilde{W}_t = \tilde{B}(\omega) Ai(t) + \tfrac{1}{2} \tilde{P}(\omega) (0 + \tfrac{1}{2}i\omega)^{-5/3} M(t), \quad (4.103)$$

where

$$M(t) = L'(t) + Ai(t)/3Ai^2(0).$$

The unknown functions  $\tilde{B}(\omega)$  and  $\tilde{P}(\omega)$  are determined from two further conditions. One is the outer boundary condition on  $\tilde{W}$ , derived from (4.99). This gives

$$\tfrac{1}{3} \tilde{B} + \frac{\tfrac{1}{2} \tilde{P}}{(0 + \tfrac{1}{2}i\omega)^{5/3}} \frac{1}{9Ai^2(0)} = \frac{\tfrac{1}{2} D''}{(i\omega)^2} \tilde{\Delta}(\omega), \quad (4.104)$$

where  $\tilde{\Delta}(\omega)$  is the Fourier transform of  $\Delta(s)$ . The other condition comes from the axial momentum equation, the last of (4.98), which was differentiated in order to arrive at (4.100). Setting  $\zeta = 0$  in the transform of this equation, we obtain

$$\tilde{W}_{\zeta\zeta}|_{\zeta=0} = i\omega \tilde{P},$$

i.e.

$$\tilde{B} Ai'(0) (0 + \tfrac{1}{2}i\omega)^{2/3} = i\omega \tilde{P} - (\tilde{P}/i\omega) (1 + Ai'(0)/3Ai^2(0)). \quad (4.105)$$

Eliminating  $\tilde{B}$  from (4.104) and (4.105), we finally obtain for the pressure transform  $\tilde{P}$ :

$$\tilde{P} = [2^{-5/3} \gamma D'' (0 + i\omega)^{-1/3} / (\omega^2 + 1)] \tilde{\Delta}(\omega), \quad (4.106a)$$

where

$$\gamma = -3Ai'(0) = 0.7765.$$

This Fourier transform, and those describing the other quantities of interest – the perturbation axial and azimuthal wall shear-rates,

$V_\zeta(0, s)$ ,  $W_\zeta(0, s)$  – can be inverted when a particular form of  $\Delta(s)$  is chosen. The shear-rate transforms are

$$\tilde{V}_\zeta(0, \omega) = \frac{2^{-4/3} \gamma D''}{3Ai(0)} \frac{(0 + i\omega)^{-2/3}}{\omega^2 + 1} \tilde{\Delta}(\omega), \quad (4.106b)$$

$$\tilde{W}_\zeta(0, \omega) = 3Ai(0) 2^{-4/3} D''(0 + i\omega)^{-5/3} \tilde{\Delta}(\omega) [1 - \gamma/9 Ai^2(0)(\omega^2 + 1)]. \quad (4.106c)$$

Before these are inverted, two general points should be made. The first is that both  $V$  and  $W$  (and hence  $v_F$  and  $w_F$ ) tend to their limits algebraically as  $\zeta \rightarrow \infty$ . In fact, they are each proportional to  $1/\zeta$ , which means that ‘slip velocities’ of  $O(Re^{-7/3})$  are generated at the edge of the inviscid core, which will drive further inviscid motions in the core at the next order in the large- $Re$  expansion. The fact that the decay of  $v_F$  and  $w_F$  is algebraic does not in this case mean that the whole theory breaks down, as it does in conventional boundary layer theory, because there is a perfectly self-consistent solution of the next-order inviscid core problem, in which the tangential velocities are singular at  $r = 1$ , but the normal velocity remains  $O(1)$ , and the pressure is also bounded (Smith, 1976c). The second general point is that (4.106) has a pole at  $\omega = -i$  in the lower half  $\omega$ -plane. This means that although there is no  $O(Re^{-2})$  perturbation in the core upstream of the curve ( $s < 0$ ), there is a significant perturbation in the boundary layer, which has to adjust itself ahead of the disturbance.

Smith (1976b) took the case (a) of uniform curvature in  $s > 0$ , so that

$$\Delta(s) = H(s) \quad \text{and} \quad \tilde{\Delta}(\omega) = 1/i\omega, \quad (4.107a)$$

where  $H(s)$  is the Heaviside step function. Other cases which it might be of interest to examine are (b) a single sharp bend in an otherwise straight tube:

$$\Delta(s) = l\delta(s), \quad \tilde{\Delta}(\omega) = l; \quad (4.107b)$$

(c) a region of uniform curvature between two straight segments at an angle:

$$\Delta(s) = H(s) - H(s - l), \quad \tilde{\Delta}(\omega) = (1 - e^{-i\omega l})/l; \quad (4.107c)$$

(d) a kink between two straight, parallel segments:

$$\Delta(s) = H(s) - 2H(s-l) + H(s-2l), \quad \tilde{\Delta}(\omega) = (1 - e^{-i\omega l})^2 / i\omega. \quad (4.107d)$$

We first consider the inversion of (4.106a, b, c) for  $s < 0$ , which requires completion of the inversion contour in the lower half-plane. The result is

$$\frac{p_F(s)}{2^{-5/3} \gamma D'' \cos \theta} = \frac{v_{F\zeta}(0, s) 3Ai(0)}{2^{-4/3} \gamma D'' \sin \theta} = -\frac{w_{F\zeta}(0, s) 3Ai(0)}{2^{-4/3} \gamma D'' \cos \theta} = \frac{1}{2} e^s \tilde{\Delta}(-i), \quad (4.108)$$

which is directly proportional to  $e^s$  in every case, and shows precisely how the upstream adjustment is made. On the wall approaching the outside of the bend ( $\theta = 0$ ) the pressure rises but the axial wall shear falls, while on the wall approaching the inside of the bend ( $\theta = \pi$ ) the opposite happens. The secondary flow is from the outside to the inside. The difference between this and what happens in a uniformly curved tube lies in the *fall* of the axial wall shear at the outside. This results from the fact that the core flow is undisturbed to this order, and the boundary layer therefore remains of uniform thickness: the boundary layer flow is effectively two-dimensional in the ' $s$ - $\theta$  plane'. The removal of fluid at  $\theta = 0$  by the secondary motions causes the axial velocity to slow down by mass conservation; the reverse is true at  $\theta = \pi$ . This sort of upstream response will also be seen in the case of unsymmetrically branched tubes (§ 5.2).

We now turn to the downstream solutions (for  $s > 0$ ). In case (a), in which  $\tilde{\Delta} = 1/i\omega$ , we invert (4.106a) to give

$$\frac{p_F(s)}{2^{-5/3} \gamma D'' \cos \theta} = \frac{1}{2\pi} \int_{-\infty}^{\infty} \frac{e^{i\omega s}}{(0 + i\omega)^{4/3}} \left[ 1 + \frac{(i\omega)^2}{1 + \omega^2} \right] d\omega.$$

The first term is evaluated using Lighthill's (1958) table 1, to give

$$[s^{1/3} / (\frac{1}{3}!)] = (3\sqrt{3}/2\pi) \Gamma(\frac{2}{3}) s^{1/3}.$$

For the second term, the contour of integration is deformed to go along both sides of the branch cut along the positive imaginary axis,

and around the pole at  $\omega = i$ . The final result is

$$p'_F = \frac{p_F(s)}{2^{-5/3} \gamma D'' \cos \theta} = \frac{3\sqrt{3}}{2\pi} \Gamma(\frac{2}{3}) s^{1/3} - \frac{1}{4} e^{-s} - \frac{\sqrt{3}}{2\pi} \int_0^\infty \frac{e^{-\xi s} \xi^{2/3}}{1 - \xi^2} d\xi, \quad (4.109)$$

where the integral assumes its principal value. This is the result obtained by Smith (1976*b*). Similarly, the following results are obtained for the correction to the axial wall shear and for the azimuthal wall shear:

$$\begin{aligned} \tau &= \frac{w_{F\zeta}|_{\zeta=0}}{2^{-4/3} \gamma D'' \cos \theta} \frac{6Ai(0)}{2^{-4/3} \gamma D'' \cos \theta} \\ &= \frac{9\sqrt{3}}{10\pi} \Gamma(\frac{1}{3}) C_1 s^{5/3} + \frac{e^{-s}}{2} - \frac{\sqrt{3}}{\pi} \int_0^\infty \frac{\xi^{-2/3} e^{-\xi s}}{1 - \xi^2} d\xi, \end{aligned} \quad (4.110)$$

$$\begin{aligned} \tau_v &= \frac{v_{F\zeta}|_{\zeta=0}}{2^{-4/3} \gamma D'' \sin \theta} \frac{6Ai(0)}{2^{-4/3} \gamma D'' \sin \theta} \\ &= \frac{3\sqrt{3}}{2\pi} \Gamma(\frac{1}{3}) s^{2/3} + \frac{e^{-s}}{2} - \frac{\sqrt{3}}{\pi} \int_0^\infty \frac{\xi^{1/3} e^{-\xi s}}{1 - \xi^2} d\xi, \end{aligned} \quad (4.111)$$

where  $C_1 = 9Ai^2(0)/\gamma - 1 > 0$ . In each case the only term to grow with distance downstream is the first, which represents the asymptotic expansion to the solution for large  $s$ . We note that the axial shear stress on  $\theta = 0$  increases with  $s$  for sufficiently large  $s$ , whereas upstream of  $s = 0$  it decreases. Hence, as with the flat entry profile, there must be a cross-over for some  $s > 0$  (in fact at  $s \approx 1.51$ ). Smith performed the integrals in (4.109)–(4.111) numerically, and fig. 4.15 shows the variation with  $s$  of the quantities evaluated, as well as two more quantities, the axial and azimuthal ‘slip velocities’ at the edge of the boundary layer, which drive the next-order core flow.

The downstream development of the flow in cases (b)–(d), where the bend is of finite length, can be calculated in a similar way. We restrict attention to the large- $s$  asymptotic expansions. In case (b), where  $\Delta(s) = l\delta(s)$ , both the pressure and the azimuthal shear stress (and hence the azimuthal velocity for all  $\zeta$ ) fall with  $s$ , while the axial

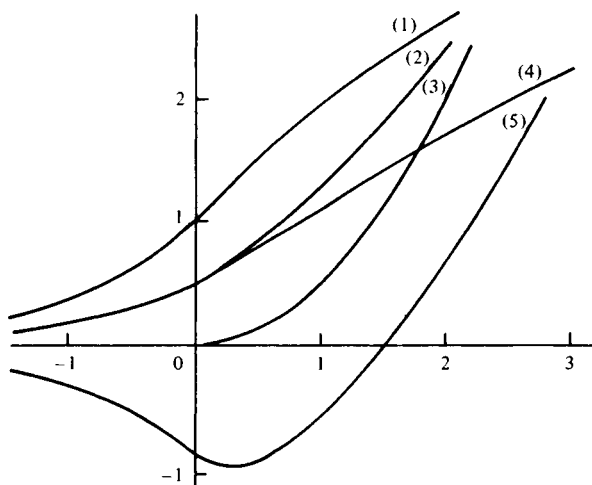


Fig. 4.15. Solution curves for the wall shear stresses and the slip velocities, axially and azimuthally. (1)  $2p'_F$ ; (2)  $v_F(s, \infty, \theta)/\sin \theta$ ; (3)  $w_F(s, \infty, \theta)/\cos \theta$ ; (4)  $\tau_v$ ; (5)  $\tau$ . (After Smith, 1976*b*.)

shear grows like  $s^{2/3}$ :

$$p'_F \sim l \frac{\sqrt{3}}{2\pi} \Gamma(\frac{2}{3}) s^{-2/3}, \quad (4.112)$$

$$\tau_v \sim l \frac{\sqrt{3}}{\pi} \Gamma(\frac{1}{3}) s^{-1/3}, \quad \tau \sim l \frac{3\sqrt{3}}{2\pi} \Gamma(\frac{1}{3}) C_1 s^{2/3}.$$

Case (c), where the bend is of finite length and, as in case (b), turns through a given angle, has exactly the same large- $s$  expansion as case (b), as one would expect. In case (d), where the tube straightens out again after a kink, even the perturbation to the axial shear falls as  $s \rightarrow \infty$ :

$$\tau \sim l^2 (\sqrt{3}/\pi) \Gamma(\frac{1}{3}) C_1 s^{-1/3}. \quad (4.113)$$

In this case alone, therefore, the presence of the bend causes no significant disturbance as  $s \rightarrow \infty$ ; this is because the effect of a bend one way is exactly cancelled out by the equal bend in the opposite sense.

The above expansion, for small  $\delta_0$  and  $s = O(1)$ , breaks down when  $s = O(\delta_0^{-1/2})$ , as can be seen either from the core flow solution (4.97) or from the fact that the boundary layer thickness is



proportional to  $Re^{1/3}s^{1/3} \propto \delta_0^{1/6}s^{1/3}$  as  $s \rightarrow \infty$  (derived from the inversion of  $\tilde{V}$  or  $\tilde{W}$  with  $\zeta \neq 0$ ). If we let  $S = \delta_0^{1/2}s$ , then the large- $s$  expansions derived above suggest that

$$\begin{aligned}w &= w_L(S, r, \theta) + O(\delta_0), \\u &= \delta_0^{1/2}u_L(S, r, \theta) + O(\delta_0^{3/2}), \\v &= \delta_0^{1/2}v_L(S, r, \theta) + O(\delta_0^{3/2}), \\p &= \bar{p}_L(S) + \delta_0 p_L(S, r, \theta) + O(\delta_0^2),\end{aligned}$$

where the separate identity of the original Poiseuille flow is lost. Substitution into the governing equations (4.1)–(4.4) shows that most terms are retained, with the exception of those describing longitudinal diffusion. Smith (1976*b*) showed that the leading term in the small- $S$  expansion is exactly the same as the leading term in the large- $s$  expansion. The problem parallels that which arises in a straight tube (§ 3.2), but numerical solution of the curved-tube equations has not been performed; presumably the fully developed solution for a given Dean number  $D'$  would result as  $S \rightarrow \infty$ .

In the case of a tube that straightens out again after a short bend, the large- $s$  problem is much simpler than in the case of constant curvature, both because the centrifugal driving force is absent, and because, at the entrance to the straight portion, the flow still represents only a small perturbation to Poiseuille flow (as long as  $l = O(1)$ ), as can be seen from (4.97). Thus it will everywhere be only a small perturbation to Poiseuille flow. In cases (b) and (c), therefore, we can write

$$\begin{aligned}w &= W_0(r) + \delta_0^{1/2}lw_M(S, r) \cos \theta + o(\delta_0^{1/2}), \\u &= \delta_0 lu_M(S, r) \cos \theta + o(\delta_0), \\v &= \delta_0 lv_M(S, r) \sin \theta + o(\delta_0), \\p &= P_0 - SD^{n-1/2} + \delta_0^{3/2}p_M(S, r) \cos \theta + o(\delta_0^{3/2}),\end{aligned}$$

while in case (d), we have

$$\begin{aligned}w &= W_0(r) + \delta_0 l^2 w_M(S, r) \cos \theta + o(\delta_0), \\u &= \delta_0^{3/2}l^2 u_M(S, r) \cos \theta + o(\delta_0^{3/2}), \\v &= \delta_0^{3/2}l^2 v_M(S, r) \sin \theta + o(\delta_0^{3/2}), \\p &= P_0 - SD^{n-1/2} + \delta_0^2 p_M(S, r) \cos \theta + o(\delta_0^2).\end{aligned}$$

The governing equations reduce in both cases to the linear forms

$$\left. \begin{aligned} u_{Mr} + \frac{u_M}{r} + \frac{v_M}{r} + w_{MS} &= 0, \\ W_0(r)u_{MS} &= -p_{Mr} + D^{n-1/2} \left( \nabla_2^2 u_M - \frac{u_M}{r^2} - \frac{2v_M}{r^2} \right), \\ W_0(r)v_{MS} &= \frac{1}{r} p_M + D^{n-1/2} \left( \nabla_2^2 v_M - \frac{v_M}{r^2} - \frac{2u_M}{r^2} \right), \\ W'_0(r)u_M + W_0(r)w_{MS} &= D^{n-1/2} \nabla_2^2 w_M, \end{aligned} \right\} \quad (4.114)$$

where  $\nabla_2^2 \equiv \partial^2/\partial r^2 + (1/r)\partial/\partial r - 1/r^2$ . The boundary conditions are  $u_M = v_M = w_M = 0$  on  $r = 1$ ,  $u_M, v_M, w_M, p_M \rightarrow 0$  as  $S \rightarrow \infty$ , and all quantities match to the large- $s$  expansions derived above as  $S \rightarrow 0$ . The three cases differ only in this upstream condition as  $S \rightarrow 0$ : in cases (b) and (c),  $w_M$  is proportional to  $S$  in the core, and  $u_M$  and  $v_M$  are independent of  $S$  there, while  $u_M$  is proportional to  $S^{1/3}$  in the boundary layer although  $v_M$  and  $w_M$  retain the same  $S$ -dependence; in case (d), all powers of  $S$  are reduced by 1. Analytical progress can be made in cases (b) and (c) by eliminating  $p_M$  from the middle two of (4.114) and by using the Laplace transform in  $S$  directly; in case (d), the initial conditions require that the variables be written as  $S^{-1}$  times new variables before the Laplace transform is applied. Because of the complexity of the initial conditions, inversion of the Laplace transform is likely to be complicated, and it may in the long run be simpler to solve the problem by a direct finite-difference integration, marching forwards in  $S$  from the initial profiles. Neither method has yet been applied.

Finally, we note that the whole linear theory for  $s = O(1)$  ceases to be valid when  $D^n = O(Re^{5/3})$ , i.e.  $\delta_0 = O(Re^{-1/3})$ , because the perturbation velocity is as large as the original Poiseuille velocity in the boundary layer, so that the boundary layer equations become non-linear and must be solved numerically. Only far upstream can one anticipate a small departure from Poiseuille flow, and there the problem reduces effectively to that which has already been solved, except that the magnitude of the perturbation, for a given  $s$ , is unknown. For example, Smith (1976*b*) shows that the pressure far

upstream must be of the form

$$p = Re^{-2/3} \beta e^s \cos(\theta + \varepsilon),$$

where  $\beta$  and  $\varepsilon$  are unknown constants that only a numerical solution can determine.